

Rate-Distortion Optimization for Transformer Inference

Anderson de Andrade, *Student Member, IEEE*, Alon Harell, *Student Member, IEEE*, Ivan V. Bajić, *Senior Member, IEEE*

Abstract—Transformers achieve superior performance on many tasks, but impose heavy compute and memory requirements during inference. This inference can be made more efficient by partitioning the process across multiple devices, which, in turn, requires compressing its intermediate representations. We introduce a principled rate-distortion-based framework for lossy compression that learns compact encodings that explicitly trade bitrate for accuracy. Experiments on language benchmarks show that the simplest of the proposed codecs achieves substantial rate savings, outperforming more complex methods. We characterize and analyze the rate-distortion behaviour of transformers, offering a unified lens for understanding performance in representation coding. This formulation extends information-theoretic concepts to define the gap between rate and entropy, and derive some of its bounds. We further develop probably approximately correct (PAC)-style bounds for estimating this gap. For different architectures and tasks, we empirically demonstrate that their rates are driven by these bounds, adding to the explainability of the formulation.

Index Terms—neural networks, rate-distortion theory, collaborative intelligence, coding for machines, learned compression, compression for machines, split computing, neural compression.

TRANSFORMER architectures [1] are predominant in many machine learning tasks. During inference, splitting the transformer architecture into manageable modules of contiguous layers allows better horizontal scaling across multiple heterogeneous devices [2], [3]. A large neural network, whose weights and intermediate states from inference do not entirely fit in a single graphical process (GPU), can be divided across multiple GPUs of similar or lower capacity. Moreover, if some devices in a cluster are not fully utilized due to monolithic constraints, splitting it across multiple devices allows to increase the cluster utilization. It is then critical that the output produced by a module is efficiently transferred to the next. For independent processes (e.g. devices) with modest bandwidth between them, this often requires that the intermediate representations be compressed before transmission. This is a common occurrence in Internet of Things (IoT) devices [4], [5]. A mobile device could perform part of the inference process, compress the intermediate representation, and then transmit it to a cloud server to complete the task.

Authors are with Simon Fraser University, 8888 University Drive, Burnaby, BC, V5S 1A6, Canada. Email communications to Anderson de Andrade: anderson_de_andrade@sfu.ca.

This work was partially funded by Intel Labs and the Natural Sciences and Engineering Research Council of Canada (NSERC).

This work has been submitted to the IEEE for possible publication. Copyright may be transferred without notice, after which this version may no longer be accessible.

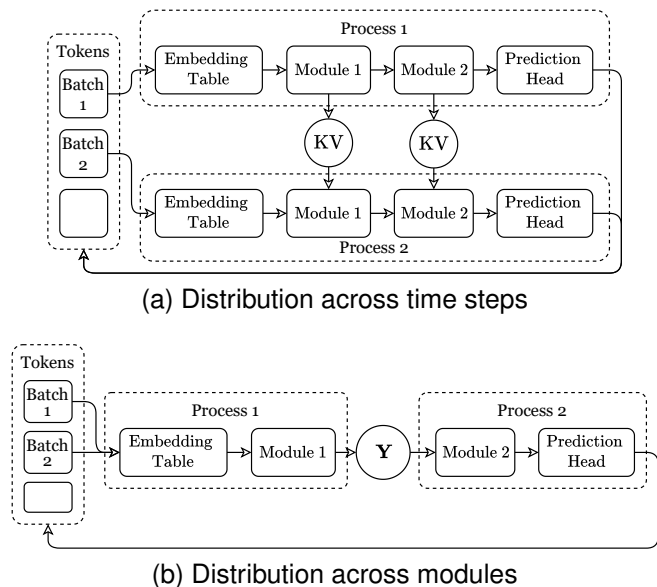


Fig. 1. Architecture diagrams for distributed transformer inference of language models (a) Replicated modules that infer different time steps require the KV cache to be transmitted. (b) If a process infers all the time steps of a module, only intermediate representations Y and the model output must be transmitted. We either assume the latter scenario, or that if the same module is replicated across time steps, the KV cache is efficiently transmitted.

In auto-regressive models such as language models, there are different ways in which the inference process can be divided between two or more devices. The same module – a contiguous subset of operations – could be deployed on multiple devices to perform inference for different time frames of a response. In such situations, the *KV cache* [1] of the module should also be transmitted. Alternatively, the same device may be responsible for all time steps of a module. In this setting, which is directly addressed by our work, only the corresponding input and output representations must be transmitted. Fig. 1 shows an overview of both configurations for language models. For language models, the transmission of token indices does not produce a significant bitrate. Their compression using existing probability models is trivial.

We propose a method (*codec*) to compress the intermediate representation produced by a transformer module. It is a *lossy* compression codec, where the target representation is optimized for a *rate* (e.g. bitrate) and a corresponding tolerable task error (*distortion*). Inherent to *learnable coding* is an *entropy model* that predicts and imposes a probability distribution on a target representation. Together with the target representation, the entropy model produces a rate that is

constrained during training. The predicted distributions from the entropy model are also used to code (compress) the target representation into a binary code and recover (decompress) the representation from such code. We propose several autoregressive entropy models based on transformers. They generate a secondary representation (*hyper-prior*) that must also be coded [6]. Focusing on language models, we benchmark their rate-distortion (RD) performance.

Due to the data processing inequality [7], the entropy of the output representation of each subsequent module can only decrease. In learnable coding, it is often expected that the rate should correlate with the entropy of the encoded representation [8]. Our empirical results show that this is not the case in transformer-based models using the evaluated entropy models, for which the rate increases as we further process the input, at equivalent distortion levels.

We explain this behavior through the theory of *usable information* [9], which takes into account the modeling power and computational constraints of an entropy model. We define and provide different bounds for \mathcal{V} -entropy and the \mathcal{V} -entropy gap – the difference between rate and entropy – and provide a generalization error bound in terms of the *Rademacher complexity* [10] of the target representation, and the *Lipschitz constant* [11] of the entropy model. We estimate some of the terms in these bounds empirically to justify observations.

The bounds on the \mathcal{V} -entropy gap explain why, due to the complexity limitations of the entropy model, the rate often operates at orders of magnitude higher than the entropy of the target representation. Moreover, the bounds of its generalization error explain why an increase in the complexity of the entropy model does not necessarily translate into better performance. This behavior is similar to the bias-variance trade-off in learning theory. We show that the \mathcal{V} -entropy gap and its generalization error can also increase with certain notions of complexity of the target representation, which, unlike its entropy, can increase in deeper layers.

I. PREVIOUS WORK

Several techniques for efficient inference of transformer architectures have been studied in the context of language models [12]. Such approaches include request batching and scheduling [13]–[17], parameter pruning [18], model quantization [19], token pruning [20], and sparse attention mechanisms [21]. The approaches in [15]–[17] share computation between multiple processes, but none consider optimizing the transferring state for rate-distortion performance.

In learnable image compression [6], [22]–[25], an *analysis transform* maps an image to a target representation. An *entropy coder* uses the probability distribution estimates from the entropy model to generate a compressed representation of the target representation. Once transferred to a secondary device, the same entropy coder and entropy model are used to recover the target representation. A *synthesis transform* maps the target representation to an approximation of the image. The methods of *coding for machines* [8], [26] generalize to other tasks in addition to image reconstruction, where the output of the system is the prediction of a machine learning task. While

these existing methods predominately work with convolutional models, in this work we focus on transformers.

In learnable coding for machines, a *task codec* is trained using an *information bottleneck* [27], [28], which is the penalization, during training, of the rate of the target representation, as provided by the entropy model. This rate reduction often results in the loss of some of the information necessary to perform a task, which increases the task distortion (error). The information bottleneck method is viewed as a method for rate-distortion optimization [7], [29].

Diverse entropy models have been proposed for learnable coding. Seminal work employed convolutional neural networks [23], [30]. More recent work uses transformer architectures [24], [31] and state-space models [32], [33]. These architectures generate a hyper-prior, which is an additional representation that must be coded and transmitted. This hyper-prior is used as *side information* for an autoregressive entropy model of the target representation. The distribution imposed on the target representation is often a multivariate normal distribution with a diagonal covariance matrix. The distribution imposed on the hyper-prior is fully-factorized and non-parametric [6]. In [34], a Fourier basis is proposed to model a fully-factorized probability distribution. Using fewer parameters, this approach is able to fit more complex distributions. In this work, we propose a relatively simple entropy model that relies heavily on the hyper-prior. We provide theoretical and empirical evidence that more complex entropy models often proposed in the literature do not offer a clear advantage for language modeling.

The rate of an *optimal* task codec is lower-bounded by the entropy of the target random variable [35]. Although there are substantial rate reductions compared to the more rate-demanding input reconstruction tasks [36], [37], to achieve optimal task performance, the resulting rate in many learnable task codecs is often orders of magnitude higher than the entropy of the target random variable. We show that the ability of a learnable codec to achieve optimality is severely limited by the complexity of both the codec and its optimization. The lowest *achievable* entropy a set of probability functions \mathcal{V} can measure in a random variable is formalized by the concept of \mathcal{V} -entropy [9]. It can be estimated with guarantees if the complexity of \mathcal{V} is bounded in terms of its *Rademacher complexity* [10]. It was shown in [9] that bounds on the complexity of \mathcal{V} directly translate to *probably approximately correct* (PAC) [38] bounds for \mathcal{V} -entropy estimation.

A. Preliminaries

This work focuses on decoder-only transformers [39]–[41] with a single coded intermediate representation, resulting in only two modules. It is straightforward to extend the proposed ideas to more modules and to encoder-decoder transformer architectures. Similarly, the proposed method could be applied to KV caches to support the distribution of the same module across multiple devices. This would allow the *compressed prefill-decode disaggregation* of language models [17], [42]. To simplify notation without loss of generalization, all transformer layers produce representations of the same dimension-

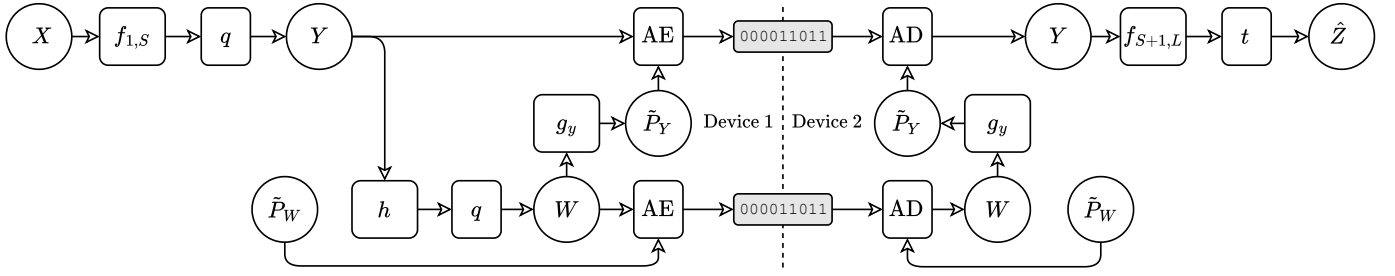


Fig. 2. Architecture overview of the proposed codec. The AE and AD blocks correspond to arithmetic encoders and decoders, respectively. They use the probability distributions provided by the entropy models to encode their target representation into a bitstream and decode it back. The dotted line separates two devices, with bitstreams (gray blocks) connecting them.

ality as the input embeddings. See the Supplementary Material for a summary of the notation used.

Assume $X \in \mathbb{R}^{T \times E}$ is an input random variable, where T is the size of a time or spatial dimension, and E is the embedding size. Let $\{f_l : \mathbb{R}^{T \times E} \rightarrow \mathbb{R}^{T \times E}\}_{l=1}^L$ be a set of L transformer blocks describing the bulk of a transformer-based neural network. The first module of the network produces the target representation as:

$$Y = (q \circ f_{1,S})(X); f_{1,S} = f_S \circ \dots \circ f_1, \quad (1)$$

where S is the *split point*, q is a *quantization function* [43]–[45], and \circ denotes the *composition operator*. This quantization (rounding) function discretizes the target representation so it can be coded. It has a differentiable training-time approximation that allows gradient propagation during automatic differentiation. The second module of the network produces the predictions as:

$$\hat{Z} = (t \circ f_{S+1,L})(Y); f_{S+1,L} = f_L \circ \dots \circ f_{S+1}, \quad (2)$$

where $t : \mathbb{R}^{T \times E} \rightarrow \mathcal{Z}$ are the header layers mapping to the sample space of the target random variable Z . A distortion function for $\hat{z}, z \sim (\hat{Z}, Z)$ is any task loss function $d(\hat{z}, z)$ such that it is bounded and non-negative.

A hyper-prior [6] is denoted as a random variable W with sample space $\mathcal{W} \subseteq \mathbb{Z}^{T \times C}$. The rate $r_w(\mathbf{w}) : \mathcal{W} \rightarrow \mathbb{R}$ of a hyper-prior $\mathbf{w} \sim W$ is the fully-factorized negative log-likelihood of a unit interval centered around \mathbf{w} [6].

Let $\Omega = \{\mathcal{W} \cup \{\emptyset\} \rightarrow \mathcal{P}(\mathcal{Y})\}$ be the set of functions that maps the side information W (e.g.: hyper-prior) or a constant \emptyset to any probability distribution over the sample space of Y . A predictive family [9] $\mathcal{V} \subseteq \Omega$ is the set of predictive models a learning algorithm is allowed to use due to computational or statistical constraints, or *rate constraints*. The predictive conditional \mathcal{V} -entropy is defined as:

$$H_{\mathcal{V}}(Y|W) = \inf_{g \in \mathcal{V}} \mathbb{E}_{\mathbf{w}, \mathbf{y} \sim W, Y} [-\log g[\mathbf{w}](\mathbf{y})]. \quad (3)$$

Setting $\mathcal{V} = \Omega$ recovers the conditional entropy measure. In addition, setting $\mathcal{W} = \emptyset$ (i.e. no side information) recovers Shannon’s entropy.

II. AN AUTO-REGRESSIVE HYPER-PRIOR IS ALL YOU NEED

Although the functions generating the hyper-prior W have access to the entire target representation Y , a rate constraint

placed on W reduces the information related to it. Hyper-priors are often used as side information by complex autoregressive entropy models that also have access to previously coded elements in the target representation Y [6], [23], [24]. This property alleviates the need for side information and can be insignificant in some cases. Hence, similarly to [6], we propose a transformer-based entropy model that does not have *direct access* to elements in Y , requiring more support from the hyper-prior.

This design choice allows to code and transmit all representation elements within a time frame in parallel. It simplifies the entropy model of the target representation by assuming full independence of its elements given the hyper-prior. In Section IV-B, we compare this method with another proposed entropy model that does not make this design choice, using previously coded elements of the intermediate representation as context. We show a relatively better performance of the former. This finding can be explained by the theory developed in Section III-C, which shows that the complexity of the entropy model increases the generalization error of the \mathcal{V} -entropy gap and this can negatively affect the rate-distortion performance of a codec.

Thus, a learnable entropy model $g_y : \mathcal{W} \rightarrow \mathcal{N}(\mathcal{Y})$; $\mathcal{W} \subseteq \mathbb{Z}^{T \times C}$, $\mathcal{Y} \subseteq \mathbb{Z}^{T \times E}$, estimates the parameters of a fully-factorized multivariate normal distribution assumed for Y , using W as the *only* context (without direct access to Y). Assuming a conditionally independent distribution for Y given W , the rate $r_y(\mathbf{y}; \mathbf{w}) : \mathcal{Y} \times \mathcal{W} \rightarrow \mathbb{R}$ for $\mathbf{y} \sim Y$ is given by the negative log-likelihood of a unit interval centered around \mathbf{y} [6]. See the Supplementary Material for concrete definitions.

A transformer-based hyper-prior model is given by:

$$W = (q \circ h)(Y); h : \mathcal{Y} \rightarrow \mathbb{R}^{T \times C}. \quad (4)$$

It is designed to enforce a dimensionality bottleneck, with each transformer block gradually decreasing the dimensions of the representation to $T \times C$. The transformer in g_y gradually increases the dimensionality to $2 \times T \times E$, where the first dimension indexes the means and variances. The change of dimensionality is done by a projection layer injected between the attention layer and the *multi-layer perceptron* (MLP) sub-block of the transformer block. Figure 2 shows a diagram of the entire codec.

Figure 3a shows a diagram of the proposed entropy models. We primarily consider the *deep factorized* density model [6] as

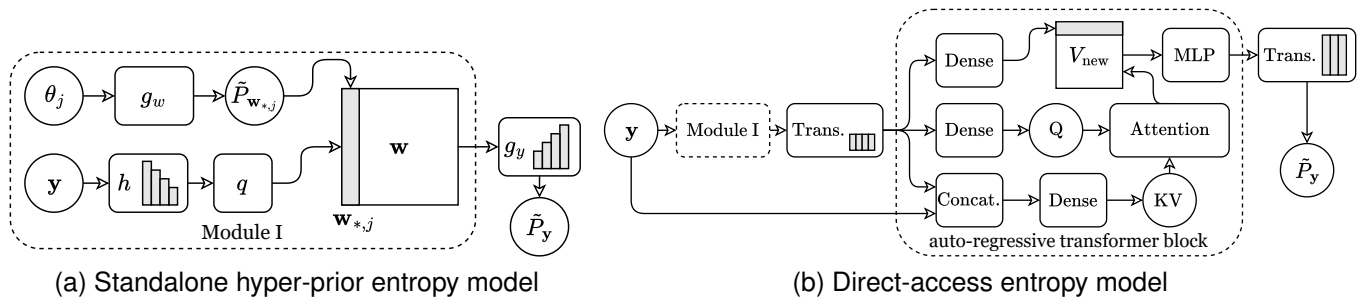


Fig. 3. Architecture diagram of the different entropy models for the target representation Y . The direct-access entropy model replaces the standalone hyper-prior entropy model with a series of transformer blocks that combine the hyper-prior and the target representation. Q, K, V corresponds to the query, key, and value embeddings in an attention mechanism. θ_j parametrizes the density function g_w that generates the probability distribution assigned to the j -th embedding dimension of W . The Fourier basis method uses the standalone hyper-prior entropy model (a) with a different density function g_w defining \tilde{P}_W .

an entropy model for the hyper-prior. It is a MLP function with a single sigmoid output parameterized by its weights, biases, and scaling factors for its activation functions. A monotonicity constraint is placed on these parameters to ensure the MLP produces valid CDFs and that the function derivatives, in this case probabilities, are always non-negative.

The masks for the attention mechanisms in h and g_y are restricted to create representations that only depend on the current and previously coded elements. Although this restriction is not required to code the hyper-prior or the target representation, it allows to grow the existing side information by only appending elements to it as the time series is further processed. This is a critical feature for auto-regressive tasks that avoids the transmission of an entire hyper-prior for the inference of a new time frame; only the new elements generated by the new time frame need to be transmitted. The attention masks ensure that:

$$\tilde{P}(\mathbf{w}|\mathbf{y}) = \prod_{i=1}^T \prod_{j=1}^C \tilde{P}(w_{i,j}|\mathbf{y}_{\leq i}), \quad (5)$$

$$\tilde{P}(\mathbf{y}|\mathbf{w}) = \prod_{i=1}^T \prod_{j=1}^E \tilde{P}(y_{i,j}|\mathbf{w}_{\leq i}), \quad (6)$$

where $\mathbf{w}_{\leq i}$ and $\mathbf{y}_{\leq i}$ correspond to the elements in these tensors from current and previous time steps, and \tilde{P} is a probability estimate implicitly established by the entropy models. As mentioned previously, another benefit of this property is that all elements within a time frame can be coded and transmitted in parallel. This has the potential to substantially reduce the inference latency due to coding.

Including the hyper-prior rate, the rate-distortion loss function is given by:

$$\mathcal{L} = \mathbb{E} \left\{ d(\hat{Z}, Z) + \lambda [r_y(Y; W) + r_w(W)] \right\}, \quad (7)$$

where $\lambda \in \mathbb{R}_+$ balances the trade-off between rate (compression) and distortion (error). The rate of the target representation r_y and the hyper-prior r_w are affected equally by λ .

III. RATE CHARACTERIZATION FOR TRANSFORMERS

Due to the determinism of the transformer, the entropy of the intermediate representations they produce can only decrease with respect to the entropy of the source (input). Hence, it is often expected that the rate of these representations will also decrease as the input is processed. We theoretically

show two situations in which this will not occur: 1) When the intermediate representations are expansions of the feature manifold representing the input; and 2) When the complexity of the intermediate representations increases so that its entropy is more difficult to model.

Both cases are orthogonal to the complexity of the entropy model. This is shown in the first case using the theory of usable information. For the second case, it is necessary to extend this theory by introducing the \mathcal{V} -entropy gap and its generalization error. The \mathcal{V} -entropy gap measures the difference between the entropy of a random variable and the optimal (i.e. for an infinite sequence) rate that an entropy model for this random variable can achieve. We show that the loss function in Eq. 7 minimizes the gap for the target representation Y under our choice of entropy model.

Since the rate of a random variable cannot be lower than its entropy, the \mathcal{V} -entropy gap factors out the entropy of the random variable, allowing us to analyze under which conditions the achievable rate of a predictive family (entropy model) can change disproportionately to the underlying entropy. Among a few different aspects, we identify that the Rademacher complexity of the target random variable can increase the generalization error of the \mathcal{V} -entropy gap.

A. The \mathcal{V} -entropy gap

We extend the theory of *usable information under computational constraints* [9] to provide the \mathcal{V} -entropy gap, a measure that captures the limitations of an entropy model to show how a rate can operate at orders of magnitude higher than the entropy of a target random variable. We provide its connection to the rate-distortion loss function and several bounds for this measure.

Definition 1. We define the \mathcal{V} -entropy gap as the absolute difference between the entropy of a random variable and the rate of an infinite coding sequence achievable by the predictive family \mathcal{V} , with both terms expressed as conditional \mathcal{V} -entropies with optional side information W :

$$G_{\mathcal{V}}(Y|W) \triangleq |H_{\mathcal{V}}(Y|W) - H_{\Omega}(Y|W)|.$$

When the side information W is \emptyset the gap can be expressed in terms of \mathcal{V} -entropies. The entropy gap can also

be interpreted as the lowest expectation of KL divergences that a predictive family can produce. See Lemma 1 in the Supplementary Material for details.

Assuming that the side information W is a function of the target representation Y , as is the case in this work, the rate terms in the loss function (Eq. 7) minimize an upper-bound over the \mathcal{V} -entropy gap of the target representation conditioned on itself while constraining the rate of W :

Theorem 1. *Let \mathcal{V}_w be a predictive family of entropy models for the hyper-prior W , and $\mathcal{V}_{g_y} \subseteq \{\mathcal{W} \cup \{\emptyset\} \rightarrow \mathcal{N}(\mathcal{Y}; \Lambda)\}$ be a predictive family of conditional entropy models g_y for the target representation, where Λ is a set of all diagonal covariance matrices. Let $\mathcal{H}(\delta); \exists h \in \mathcal{H}(\delta) : W = (q \circ h)(Y)$ be a set of constrained hyper-prior functions such that $H_{\mathcal{V}_w}(W) \leq \delta, \delta \geq 0$. Defining a constrained predictive family $\bar{\mathcal{V}}_y = \mathcal{H}(\delta) \times \{q\} \times \mathcal{V}_{g_y}$, we have that:*

$$G_{\bar{\mathcal{V}}_y}(Y|Y) = H_{\bar{\mathcal{V}}_y}(Y|Y) \leq \min \mathbb{E} [r_y(Y; W) + r_w(W)],$$

where the minimum is over the unconstrained predictive families $\mathcal{V}_y = \mathcal{H}(\infty) \times \{q\} \times \mathcal{V}_{g_y}$, and \mathcal{V}_w .

Proof. See the Supplementary Material.

The predictive family $\bar{\mathcal{V}}_y$ subsumes the hyper-prior model h together with the entropy model g_y . We adapt this theorem to our method by restricting the predictive family $\bar{\mathcal{V}}_y$ so that it only produces multivariate normal distributions with diagonal covariances. This result allows us to interpret part of the rate-distortion optimization problem as directly minimizing a \mathcal{V} -entropy gap. The rate restriction placed on W , in addition to the potential limitations of the predictive families, prevents this \mathcal{V} -entropy gap from always reaching zero. In fact, for it to be zero, all information about Y must be present in W in such a way that it can be coded at a rate equal to or lower than if it were to be coded in Y unconditionally. Hence, there is a trade-off between the rate of the hyper-prior and the conditional rate of the target representation.

We derived bounds on the \mathcal{V} -entropy gap showing interesting relationships between the Lipschitz constants of the functions involved. If we have side information that originates from a common ancestor with the target random variable, we have the bound shown by Theorem 5 in the Supplementary Material. If W is a function of the target representation Y , as is the case in the proposed entropy models, we have the bound in Theorem 6 of the Supplementary Material.

B. Expansions of the feature space

In learnable compression, the target representations and hyper-priors are often treated as continuous random variables for which we assign continuous distributions that we then quantize (discretize). Due to this fundamental choice, the stretch factor of the functions generating these representations can affect the \mathcal{V} -entropy of these random variables independently of the choice of predictive family (entropy model).

The differential entropy of a continuous variable is not invariant under change of variables. Moreover, the entropy of a quantized random variable upper-bounds the differential entropy of the continuous variable for sufficiently small

quantization steps. Thus, for a target representation Y , the conditional \mathcal{V} -entropy gap can be upper-bounded by an expression that involves the covariance determinant of the target representation:

Theorem 2. *Let $\mathcal{V} \subseteq \Omega$ be a predictive family according to [9], and $Y = q(Y'; \Delta)$ the quantization of a continuous random variable with $\text{cov}(Y') = \Sigma$, where Δ is the maximum quantization step. Then, with $D = |Y| = T \times E$, we have:*

$$H_{\mathcal{V}}(Y|W) \leq 1/2 \log \det \Sigma + D/2 \log (2\pi e) \\ + G_{\mathcal{V}}(Y|W) - \log \Delta \quad \text{as } \Delta \rightarrow 0.$$

Proof. See the Supplementary Material.

Many quantizers used in learnable coding have a fixed quantization step $\Delta = 1$, which effectively rounds values to their closest integer. With $\Delta = 1$, the provided bound is an approximation. However, the relationship between Shannon's entropy and differential entropy used for this bound is commonly used empirically, for relatively large values of Δ , with compelling results [7]. If the target representation is a discrete random variable and is treated as such, there would be no impact from its covariance on the \mathcal{V} -entropy since it would be dimensionless.

In Section IV-D, we measure an approximation of the covariance determinant of the target representations of different neural network layers. This quantity in Theorem 2 is independent of the capacity of the entropy model, which remains fixed across layers in the experiments, and is captured by the \mathcal{V} -entropy gap. We show a positive correlation between the covariance determinant and the rate, providing one reason why deeper layers can exhibit higher rate.

A more obvious result shows how the Lipschitz constant – a direct measure of the dilation of a function [11] – of the function generating the target representation can increase its \mathcal{V} -entropy:

Theorem 3. *Let $\mathcal{V} \subseteq \Omega$ be a predictive family according to [9], and $Y = q(Y'; \Delta)$ the quantization of a L_f -Lipschitz function of a continuous random variable X such that $Y' = f(X)$, with $\text{cov}(Y') = \Sigma$, where Δ is the maximum quantization step. Then, with $D = |Y| = T \times E$, we have:*

$$H_{\mathcal{V}}(Y|W) \leq h(X) + D(L_f - 1) \\ + G_{\mathcal{V}}(Y|W) - \log \Delta \quad \text{as } \Delta \rightarrow 0.$$

Proof. See the Supplementary Material.

C. Generalization bounds for the \mathcal{V} -entropy gap

In practice, we often use a set of samples to minimize the \mathcal{V} -entropy gap, since the joint distribution of the target representation and side information $P_{Y,W}$ is not known. Learning theory [10] establishes the generalization error to be the hypothesis (e.g.: model parameters) producing the largest error between the expectation of its outputs and a corresponding empirical measure. This quantity can usually be bounded by the complexity of the hypothesis family (model architecture). Intuitively, a hypothesis family with a smaller complexity is easier to learn.

Analog results exist for \mathcal{V} -entropy, where the complexity of the predictive family \mathcal{V} results in probably approximately correct (PAC) [10] bounds for \mathcal{V} -entropy estimation. We define the generalization error for the \mathcal{V} -entropy gap and establish similar bounds.

Definition 2. Let $\mathcal{D} = \{(\mathbf{y}_i, \mathbf{w}_i)\}_{i=1}^N \sim Y, W$ be a set of samples. We define the generalization error of the \mathcal{V} -entropy gap as:

$$R_{\mathcal{V}, \mathcal{D}}(Y|W) \triangleq \left| G_{\mathcal{V}}(Y|W) - \inf_{g \in \mathcal{V}} \frac{1}{N} \sum_{(\mathbf{y}, \mathbf{w}) \in \mathcal{D}} \log \frac{P_{Y|W}(\mathbf{y}|\mathbf{w})}{g[\mathbf{w}](\mathbf{y})} \right|.$$

This term can be upper-bounded in terms of the Rademacher complexity [10] of the target representation and the Lipschitz constant of the predictive family \mathcal{V} :

Theorem 4. Let $\mathcal{V} \subseteq \Omega$ be a predictive family according to [9], Y and W random variables with sample spaces \mathcal{Y} and \mathcal{W} , respectively, with $\mathcal{D} = \{(\mathbf{y}_i, \mathbf{w}_i)\}_{i=1}^N \sim Y, W$ as a set of samples. Assume that $\forall g \in \mathcal{V}, \mathbf{y} \in \mathcal{Y}, \mathbf{w} \in \mathcal{W}, \log g[\mathbf{w}](\mathbf{y}) \in [-B, B], \log P_{Y|W}(\mathbf{y}|\mathbf{w}) \in [-B, B]$, and that the Lipschitz constant of $P_{Y|\mathbf{w}} \forall \mathbf{w} \in \mathcal{W}$ is governed by the Lipschitz constant of a multivariate normal distribution with covariance matrix αI , such that $\alpha \leq \exp(2BD^{-1})(2\pi)^{-1}$. Then, $\forall \delta \in (0, 1)$, with probability at least $1 - \delta$, we have:

$$R_{\mathcal{V}, \mathcal{D}}(Y|W) \leq 2 \left[(\text{Lip}(\mathcal{V}_r) + \beta) \text{Rad}(\mathcal{D}) + B \sqrt{2/N \log 1/\delta} \right],$$

where $\text{Rad}(\mathcal{D})$ is the Rademacher complexity of the concatenated samples in the dataset \mathcal{D} , $\text{Lip}(\mathcal{V}_r)$ is the maximum Lipschitz constant in $\mathcal{V}_r = \{v|v(\mathbf{w}, \mathbf{y}) = \log g[\mathbf{w}](\mathbf{y}), g \in \mathcal{V}\}$, and:

$$\beta \triangleq \alpha^{-1/2} [2B - D \log(2\pi\alpha)]^{1/2}.$$

Proof. See the Supplementary Material.

This result shows that the generalization error of the \mathcal{V} -entropy gap is upper-bounded by the Rademacher complexity of a set of target representations. As the set \mathcal{D} grows in size (samples), the Rademacher complexity and the second term decrease, minimizing the generalization error. β captures the complexity of an assumed multivariate normal probability distribution $P_{Y|W}$. For $R_{\mathcal{V}, \mathcal{D}}(Y|Y)$ we have that $\beta = 0$.

In Section IV-D, we measure an approximation of the Rademacher complexity of the target representations of different neural network layers. This quantity is present in Theorem 4, along with other terms that remain constant across layers. We show a positive correlation between this quantity and the rate achieved on the target representations. This provides further reasoning as to why the rate might not correlate with the entropy of the target representations.

IV. EXPERIMENTAL RESULTS

We evaluate the rate-distortion performance of the proposed architecture on language modeling. The results are compared between the deep factorized method and a method that uses Fourier basis functions [34] for the density estimation of the hyper-prior. In addition, we compare with a *direct-access* auto-regressive entropy model that has access to previously coded

elements of the target representation and not just the hyper-prior, which contains overall only a subset of the information in the target representation. Figure 3 shows an overview of the two entropy models.

We train codecs with different values of λ at multiple split points to obtain rate-distortion curves. The results show that under similar distortion performance, the \mathcal{V} -entropy gap increases with the split point. We attribute this behavior to an increase in the \mathcal{V} -entropy gap, as well as its generalization error, demonstrated by increases in the covariance determinant and Rademacher complexity of the target representation through the network. This behavior is evaluated in other architectures and modalities, such as residual neural networks and images. All results are reported for validation sets. The official code is available at github.com/adeandrade/research.

A. Architecture of the entropy models

The hyper-prior model h is composed of 4 transformer blocks that sequentially bring down the embedding space E to 384, 192, 96, and finally, $C = 24$ dimensions. Following [46], the dense layers in the transformer blocks have no biases, and the different sub-components have residual connections and layer normalizations. The deep factorized entropy model uses 9 dense layers with 3 hidden dimensions, for a total of 118 parameters per dimension in C . The entropy models for the target representation g_y is composed of another 4 transformer blocks, that sequentially bring up the embedding space to 96, 192, 384, and finally, E dimensions. To quantize Y and W , q is set as a conventional integer rounding operation, where, during automatic differentiation, the incoming gradients are passed to the next operation as they were [44].

In the method using a Fourier basis density model, the assumed PDF for each dimension of the hyper-prior is independently modeled as a Fourier series with a finite number of coefficients [34]. To ensure non-negativity of the PDF, the coefficients are auto-correlated, making the Fourier series positive semi-definite. The function over one period is divided by its integral for normalization, and has a closed-form solution. The resulting periodic density function is extended to the entire real line by a learnable mapping $(-1, 1) \rightarrow \mathbb{R}$ parameterized by a scaling and an offset learnable parameter.

The Fourier coefficients are learned while training the proposed loss function. We used 60 coefficients for a total of 120 parameters when counting the real and imaginary components. This number is similar to the number of parameters used in the deep factorized density model. The hyper-prior W is quantized using the same approach in the deep factorized method.

In the direct-access entropy model, an auto-regressive transformer predicts the means and variances of the target representation using the hyper-prior *and the previous elements in the time series* of the target representation. The hyper-prior W is used as query embeddings and additional dimensions for the key and value embeddings of the attention mechanism in an initial transformer block. The auto-regressive restriction allows the entropy model to be used for coding since the serialized decoding process only has access to previously-decoded elements.

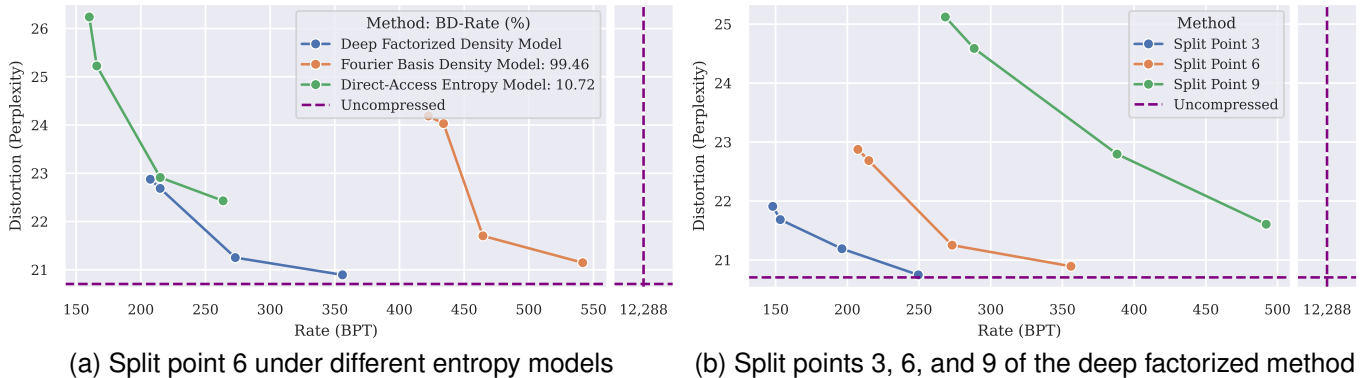


Fig. 4. Rate-distortion performance for GPT-2. The rate is measured in bits-per-token (BPT). Perplexity is the exponent of the classification cross-entropy loss, used as distortion. *Uncompressed* is a model with no quantization or rate penalty ($\lambda = 0$), which uses 16 bits per token element. The standalone hyper-prior entropy model using the deep factorized density method outperforms the other entropy models. Its rate-distortion performance decreases with the split point.

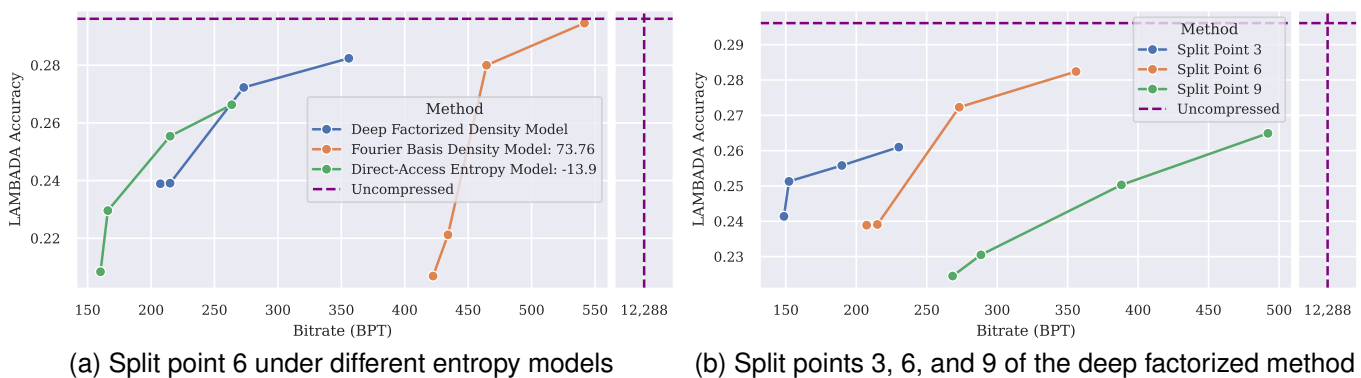


Fig. 5. Rate-performance for GPT-2 evaluated on the the LAMBADA language task. The rate is measured in bits-per-token (BPT). *Uncompressed* is a model with no quantization or rate penalty ($\lambda = 0$).

Figure 3b presented an overview of the direct-access entropy model architecture. Using the same hyper-prior architecture with the deep factorized density model, the entropy model for the target representation first passes the hyper-prior through 4 transformer blocks with causal attention masks that maintain the same embedding size C . The resulting tensor is then processed by a custom transformer block in which, for each role, a single dense layer produces: 1) Query embeddings of C dimensions; 2) Key and value embeddings of size C and E respectively, as a function of the target embeddings and this tensor; and 3) The value embedding of the first time step after attention. This transformer block uses an attention mask that prevents access to elements from the current time step forward. The output of the transformer block is then further processed by 3 more transformer blocks that use causal attention masks and retain the same embedding size E , except for the last block, which increases the output embedding size to $2E$. The output tensor is split into the means and variances of the multivariate normal distribution for Y .

B. Rate-distortion performance benchmarks

We use the GPT-2 Small [47] transformer architecture as a language model. It has $L = 12$ transformer blocks with 12 attention heads and embeddings of $E = 768$ dimensions, resulting in 124 million parameters. As an auto-regressive

language task, we use the OpenWebText [48] dataset, mainly comprised of Reddit conversation threads.

The loss function is given by Eq. 7. Different values of λ produce different points on the rate-distortion curve. The 6th transformer block was chosen as the split point. See the Appendix and the Supplementary Material for more details and other results, including a detailed description of the comparative methods previously introduced.

Figure 4a shows the rate-distortion curves obtained under the different entropy models. The rate reported is the sum of the individual rates of the hyper-prior and target representations. The Fourier basis and direct-access entropy model methods have an increase in rate, measured by BD-rate [49], of 99.46% and 10.7%, respectively, with respect to the deep factorized density method. Thus, the simpler model outperforms the other more complex proposed methods. Interestingly, the Fourier basis method uses much more bits for the hyper-prior.

A more interpretable task metric for a language model is LAMBADA [50], which evaluates the ability to comprehend context and understand discourse. We score the language models created in Section IV-B using this method. Since the language models have not been trained further for question-answering tasks, we strip all prompting, making no distinction between context and target sentences, and use the first word

TABLE I
GPU CODEC PERFORMANCE

Codec	Rate (BPT)	Rate (%)	Time (μ SPT)	W2W (μ SPT)
<i>Rate-constrained</i>				
Proposed	292	2.38	3.90	6.82
GDeflate	7,005	57.01	45.18	115.23
Zstd	3,843	31.27	52.02	90.45
<i>Unconstrained</i>				
Raw	12,288	100.00	0	122.88
GDeflate	14,327	116.59	45.55	188.82
Zstd	12,727	103.57	50.63	177.90

TABLE II
CPU CODEC PERFORMANCE

Codec	Rate (BPT)	Rate (%)	Time (μ SPT)	W2W (μ SPT)
<i>Rate-constrained</i>				
Proposed	292	2.38	26.42	29.34
Deflate	2,187	17.80	15.09	36.96
Zstd	2,818	22.93	12.49	40.67
<i>Unconstrained</i>				
Raw	12,288	100.00	0	122.88
Deflate	11,938	97.15	14.07	133.45
Zstd	11,852	96.45	12.40	130.92

produced after stripping punctuation.

Figure 5a shows the rate-performance of the methods presented in this work. There is some missing overlap between the curves, which makes the BD-rate measurements unreliable. With that in mind, there is a rate reduction of 13.9% for the direct-access entropy method compared to the deep factorized method. The Fourier basis density model has a rate increase of 73.76% over the deep factorized density model.

Figure 5b shows the rate-performance at different split points of the standalone hyper-prior entropy model with a deep factorized density. Interestingly, some points for the split point $S = 6$ have the best overall LAMBADA accuracies.

C. Bitrate and time comparisons

We compare the proposed codec with Deflate [51] and Zstandard (Zstd) [52], which are lossless data compression algorithms commonly used for tensors. We choose the deep factorized model from Section IV-B with the lowest perplexity (highest bitrate) under split point $S = 3$. The rate and time produced by the codecs are evaluated on both CPUs and GPUs under heavy parallelization, as is often the case for inference services, so that the response throughput is maximized. In the CPU benchmarks, the inference on the hyper-prior used a GPU and the rest of the coding algorithm ran on a CPU. See the Supplementary Material for more details and benchmark settings.

Table I and Table II show the codec performance results for GPUs and CPUs, respectively. In the *Rate-constrained* set of experiments, the baseline methods use the rate-constrained representations from the proposed method. The *Unconstrained* methods correspond to the compression of unconstrained representations from a vanilla GPT-2 model. The *Raw* method

just transmits an uncompressed representation at 16 bits per value, since it uses the *bfloat16* floating-point format. For GPU benchmarks, GDeflate [53], a variant of Deflate optimized for GPUs. The coding time measurements are reported in microseconds per token (μ SPT) and the wall-to-wall (W2W) measurements assume an effective link speed of 100 Mbps and no protocol overhead.

The rate of the proposed codec is substantially lower than the benchmarks. Moreover, compressing the rate-constrained representations produced by our analysis transforms using off-the-shelf lossless codecs seems to have significant advantages in both rate and time over unconstrained representations. This result shows that even if we opt to use an off-the-shelf codec, there is still a significant benefit in using the rate-constrained representations induced by the proposed methods.

In GPU benchmarks, the proposed method outperforms baselines in both rate and time. On the CPU, Zstandard, which uses the same dictionary-matching algorithm as DEFLATE, produces higher rates but is considerably faster than the other methods. However, we believe that our current implementation could be substantially optimized. The inference time of the entropy model on the GPU is 4.35% of the total coding time. This places most of the current time overhead on the entropy codec. Using *tabled ANS* (tANS) [54], a variant of an asymmetric numeral system (ANS), could help close the time performance gap, as it is the entropy coder used in the faster Zstandard method [52]. However, this change would most likely result in higher memory consumption. Nevertheless, compared to the Zstandard codec applied to our rate-constrained representations, at the current coding speed, and assuming a communication protocol overhead of 9% [55], the proposed codec is more efficient when the effective link speed is less than 197.66 Mbps.

D. Rate-distortion performance and the split point

Figure 4b shows the rate-distortion performance for 3 equidistant split points S of the standalone hyper-prior entropy model with a deep factorized density. Compared to the uncompressed method, some of the codecs have minimal impact on task performance and operate at a rate that is an order of magnitude lower.

The results also show an increase in rate-distortion as the split point is placed further from the source. This behavior could be unexpected since, the transformer being deterministic, the entropy of the processed input can only decrease. However, it is often observed in the context of coding for machines that rates operate at orders of magnitude higher than the theoretical bounds for the entropy of the target [35]. This behavior can be explained by an increase in the \mathcal{V} -entropy and the generalization error of the \mathcal{V} -entropy gap of the target representation, as established in Section III. Intuitively, as the source is further processed by non-linear functions in a high-dimensional space, the dilation and complexity of the intermediate representations increases, making their entropy higher and probability density more difficult to estimate.

To demonstrate this, we perform experiments in which, for different tasks and model architectures, we introduce a rate

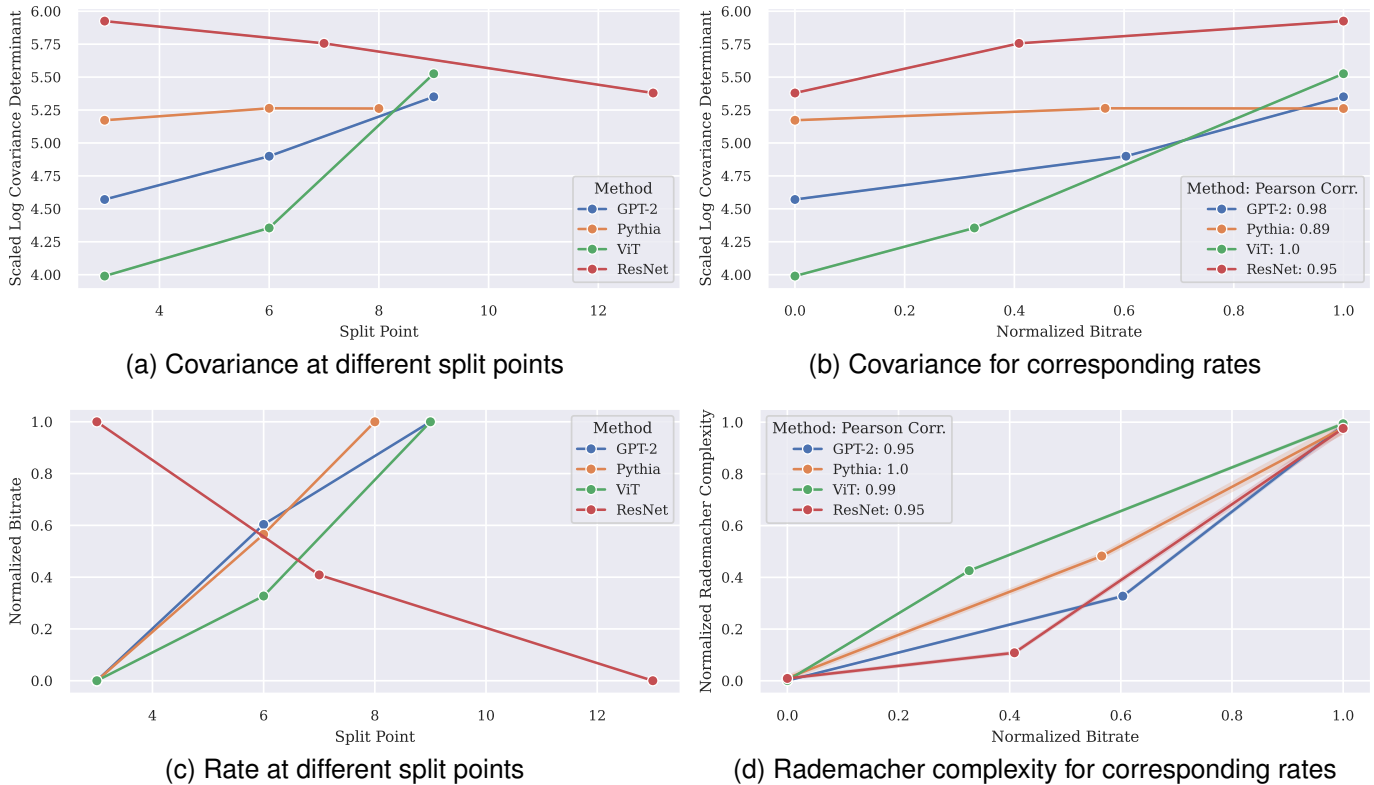


Fig. 6. Rate, covariance determinant, and Rademacher complexity estimates at different split points, for GPT-2 Small, Pythia 160M, ViT B/16, and ResNet 34. Some axes are min-max scaled per method to facilitate comparison. The logarithmic scale is further scaled by $1/2D$. The Rademacher complexity and covariance determinant strongly correlate with rate. Only in ResNets, the rate-distortion performance increases with the split point. Very narrow bands show the standard deviation of the covariance determinant and Rademacher complexity measures over 10 samples.

constraint at different split points, measure the rate obtained by the proposed entropy model, and compare it with estimates of the covariance determinant and the Rademacher complexity of the target representation. These two quantities are part of the \mathcal{V} -entropy bound in Theorem 2 and the generalization bound in Theorem 4, respectively. The entropy model architecture, settings, and the optimization algorithm, are fixed across experiments, ensuring that the Lipschitz constant of the predictive family \mathcal{V}_r acts as a constant in Theorem 4. We also estimate and compare the Lipschitz constants of the entropy models obtained, for further analysis.

We establish 4 methods for comparison: 1) The GPT-2 Small language models from Section IV-B; 2) Language models using the Pythia 160M architecture [56]; 3) A transformer-based image classification task using ViT B/16 [57]; and 4) A convolutional neural network image classification task using ResNet 34 [58]. The goal behind these choices is to pinpoint which aspects (i.e., model architecture, modality) produce a decrease in rate-distortion performance in deeper information bottlenecks, and to evaluate the correlation between the rate and its bounds in these diverse scenarios. See the Supplementary Material for more details on the comparative methods, as well as an analysis of the Lipschitz constants.

1) *Covariance determinant of the target representation:* we compute an approximation of the covariance determinant of the target representation Y using the eigenvalues of the Hessenberg matrix produced by 1,000 Arnoldi iterations [59]

over $N = 1,000$ samples, with context size $T = 512$. The procedure is similar to the more practical Restarted Arnoldi iteration method, popularized by the ARPACK software package [60]. The Arnoldi iteration algorithm produces an orthogonal basis for the Krylov subspace for a target matrix A , which is the linear subspace spanned by the images of a random vector b under powers of A [61]. The method also produces a Hessenberg (almost triangular) matrix [62] with the dot products of the vectors of this orthogonal basis. It is often observed that the eigenvalues of this Hessenberg matrix converge to eigenvalues of the original matrix A . We use this subset of eigenvalues as an estimation of the covariance determinant of the target representation.

Typically, the eigenvalues obtained from the suggested approach correspond to the larger eigenvalues of the input matrix. Obtaining the smaller eigenvalues involves the inversion or pseudo-inversion of the input matrix. Due to the size of the target representations Y , an inversion is not tractable. Moreover, due to the deduced large condition number of $\text{Cov}(Y)$, a pseudo-inversion is not reliable as the procedure is often numerically unstable. Despite the bias in the proposed estimate, with a sufficiently large subset of eigenvalues, it appears adequate for assessing trends in the magnitude of the covariance determinant.

2) *Rademacher complexity of the target representation:* to estimate the Rademacher complexity of the target representation, we replace the Rademacher random variable expectation

in its definition with an empirical measure, obtaining:

$$\bar{\text{Rad}}(\mathcal{D}) = \frac{1}{MN} \sum_{\mathbf{a} \in \mathcal{A}} \max_{i=1}^T \max_{j=1}^E \left(\left| \sum_{k=1}^N a_k \mathcal{D}_k \right| \right)_{i,j}, \quad (8)$$

where \mathcal{D}_k indexes the samples of Y , and $\mathcal{A} = \{\mathbf{a}_i\}_{i=1}^M \sim A$, where A is a random variable with sample space $\{-1, 1\}^N$ following the Rademacher distribution. We set $N = 1,000$, $M = 10,000$ and the context size to $T = 512$. Replacing the expectation in the Rademacher complexity with their empirical estimates has been explored before in [63]. The Rademacher complexity estimates have relatively low variance and does not significantly change the Pearson correlation coefficients.

Since our estimate of Rademacher complexity reacts to changes in dimensionality, the measure for the ResNet method is performed on the output of the convolution layer prepended to the entropy model, which has the same dimensionality across split points. The target representation is quantized before computing the Rademacher complexity and covariance determinant estimates.

3) *Results:* figure 6a shows estimates of the covariance determinant of the target representation per split point, with strong correlations. Figure 6b shows the relationship between the covariance determinant of the target representation and the bitrate obtained by the proposed entropy model. The average Pearson correlation between these two measurements is 0.96. The strong correlation corroborates the increase in rate as the split point S is placed further.

Figure 6c shows the change in rate as a function of the split point. For all transformer models, the rate increases with depth, whereas for the ResNet model, the inverse occurs. Figure 6d shows the estimate of the Rademacher complexity and compares it with the rate of the target representation. There is a strong Pearson correlation, with an average of 0.97.

V. SUMMARY AND CONCLUSION

We propose several lossy compression methods for the auto-regressive coding of intermediate representations of a transformer. The \mathcal{V} -entropy theory is extended by introducing the \mathcal{V} -entropy gap. For our architecture, we tied this concept to the rate of our proposed loss. We presented bounds on the \mathcal{V} -entropy and \mathcal{V} -entropy gap under diverse configurations of the side information, giving us insight into why these quantities can increase. In addition, PAC-like bounds are presented for the generalization error of the \mathcal{V} -entropy gap. Together, these results extend the theory for rate-distortion optimization.

A commensurate increase in the complexity of the entropy model to meet the requirements of a target representation could result in a decrease in the \mathcal{V} -entropy gap. However, this positive contribution is offset by an increase in the generalization error. An increase in this generalization error might explain why the more complex entropy models proposed in this work do not perform as well as the simplest of the proposed entropy models, which outperforms them by at least 10.7%.

We present a rate-time performance analysis that justifies the value of rate constraints for the compression of transformer representations. We show that there is a significant advantage

in using the proposed codec on GPUs. For CPUs, our proposed codec outperforms the baselines when, under minor assumptions, the effective link speed is less than 197.66 Mbps.

We see that for transformers using one of the proposed entropy models, the rate-distortion performance decreases as we code the intermediate representations from deeper layers. This behavior is justified by an increase in the covariance determinant and the Rademacher complexity of the target representation, concepts that bound \mathcal{V} -entropy and the generalization error of the \mathcal{V} -entropy gap, respectively. Only for the ResNet task considered, the rate decreases in deeper layers, yet we still find that both the covariance determinant and Rademacher complexity of the target representations positively correlate with rate. This transformer trait seems to be required to perform the tasks at a similar distortion level across split points. In fact, we report that our experiments using methods that constrain the Lipschitz constant of the function generating the target representation – a bound over both the covariance determinant and the Rademacher complexity of the target representation and consequently its rate – result in language models for which training does not effectively reduce the task objective. This corroborates the results of [64], where, to match the validation accuracy of NanoGPT [46], the constant of a Lipschitz-constrained transformer had to increase to 10^{264} .

The better rate-distortion performance of earlier split points is advantageous in the Internet of things (IoT) domain, where resource-constrained edge devices can only perform the first few inference steps. Powerful devices on the cloud would then perform the rest of the inference process. Conveniently, transmitting representations from an early split point using the proposed method would result in better rate-distortion performance while also accommodating to these resource constraints.

REFERENCES

- [1] A. Vaswani, N. Shazeer, N. Parmar, J. Uszkoreit, L. Jones, A. N. Gomez, L. Kaiser, and I. Polosukhin, "Attention is all you need," in *NeurIPS*, 2017.
- [2] M. A. Maruf, A. Azim, N. Auluck, and M. Sahi, "Optimizing DNN training with pipeline model parallelism for enhanced performance in embedded systems," *JPDC*, 2024.
- [3] M. R. Jafari, J. Su, Y. Zhang, O. Wang, and W. Zhang, "PiSeL: Pipelining DNN inference for serverless computing," in *ACM CIKM*, 2024.
- [4] Y. Matsubara, M. Levorato, and F. Restuccia, "Split computing and early exiting for deep learning applications: Survey and research challenges," *ACM Computing Surveys*, 2023.
- [5] H. Ko, H. Jeong, D. Jung, and S. Pack, "Dynamic split computing framework in distributed serverless edge clouds," *IEEE IoTJ*, 2024.
- [6] J. Ballé, D. Minnen, S. Singh, S. J. Hwang, and N. Johnston, "Variational image compression with a scale hyperprior," in *ICLR*, 2018.
- [7] T. M. Cover and J. A. Thomas, *Elements of information theory (Second edition)*. Wiley, 2006.
- [8] H. Choi and I. V. Bajic, "Scalable image coding for humans and machines," *IEEE TIP*, 2022.
- [9] Y. Xu, S. Zhao, J. Song, R. Stewart, and S. Ermon, "A theory of usable information under computational constraints," in *ICLR*, 2020.
- [10] S. Shalev-Shwartz and S. Ben-David, *Understanding machine learning - from theory to algorithms*. Cambridge University Press, 2014.
- [11] Y. Benyamini and J. Lindenstrauss, *Geometric Nonlinear Functional Analysis*. American Mathematical Society, 2000.

- [12] M. Xu, W. Yin, D. Cai, R. Yi, D. Xu, Q. Wang, B. Wu, Y. Zhao, C. Yang, S. Wang, Q. Zhang, Z. Lu, L. Zhang, S. Wang, Y. Li, Y. Liu, X. Jin, and X. Liu, "A survey of resource-efficient LLM and multimodal foundation models," *ArXiv*, vol. 2401.08092, 2024.
- [13] G. Yu, J. S. Jeong, G. Kim, S. Kim, and B. Chun, "Orca: A distributed serving system for transformer-based generative models," in *USENIX OSDI*, 2022.
- [14] A. Agrawal, N. Kedia, A. Panwar, J. Mohan, N. Kwatra, B. S. Gulavani, A. Tumanov, and R. Ramjee, "Taming throughput-latency tradeoff in LLM inference with Sarathi-Serve," in *USENIX OSDI*, 2024.
- [15] Y. Sheng, L. Zheng, B. Yuan, Z. Li, M. Ryabinin, B. Chen, P. Liang, C. Ré, I. Stoica, and C. Zhang, "FlexGen: High-throughput generative inference of large language models with a single GPU," in *ICML*, 2023.
- [16] J. He and J. Zhai, "Fastdecode: High-throughput GPU-efficient LLM serving using heterogeneous pipelines," *ArXiv*, vol. 2403.11421, 2024.
- [17] P. Patel, E. Choukse, C. Zhang, A. Shah, Í. Goiri, S. Maleki, and R. Bianchini, "Splitwise: Efficient generative LLM inference using phase splitting," in *ISCA*, 2024.
- [18] M. Zhang, H. Chen, C. Shen, Z. Yang, L. Ou, X. Yu, and B. Zhuang, "LoRAPrune: Structured pruning meets low-rank parameter-efficient fine-tuning," in *ACL*, 2024.
- [19] J. Lin, J. Tang, H. Tang, S. Yang, W. Chen, W. Wang, G. Xiao, X. Dang, C. Gan, and S. Han, "AWQ: Activation-aware weight quantization for on-device LLM compression and acceleration," in *MLSys*, 2024.
- [20] H. Jiang, Q. Wu, C. Lin, Y. Yang, and L. Qiu, "LLMLingua: Compressing prompts for accelerated inference of large language models," in *EMNLP*, 2023.
- [21] I. Beltagy, M. E. Peters, and A. Cohan, "Longformer: The long-document transformer," *ArXiv*, vol. 2004.05150, 2020.
- [22] J. Ballé, V. Laparra, and E. P. Simoncelli, "End-to-end optimized image compression," in *ICLR*, 2017.
- [23] D. He, Z. Yang, W. Peng, R. Ma, H. Qin, and Y. Wang, "ELIC: efficient learned image compression with unevenly grouped space-channel contextual adaptive coding," in *CVPR*, 2022.
- [24] R. Zou, C. Song, and Z. Zhang, "The devil is in the details: Window-based attention for image compression," in *CVPR*, 2022.
- [25] W. Jiang, J. Yang, Y. Zhai, F. Gao, and R. Wang, "MLIC++: Linear complexity multi-reference entropy modeling for learned image compression," *ACM TMCCA*, 2025.
- [26] A. Harell, A. de Andrade, and I. V. Bajic, "Rate-distortion in image coding for machines," in *PCS*, 2022.
- [27] N. Tishby, F. C. N. Pereira, and W. Bialek, "The information bottleneck method," in *Allerton Conference*, 1999.
- [28] N. Friedman, O. Mosenzon, N. Slonim, and N. Tishby, "Multivariate information bottleneck," in *UAI*, 2001.
- [29] M. I. Belghazi, A. Baratin, S. Rajeswar, S. Ozair, Y. Bengio, R. D. Hjelm, and A. C. Courville, "Mutual information neural estimation," in *ICML*, 2018.
- [30] W. Jiang, J. Yang, Y. Zhai, P. Ning, F. Gao, and R. Wang, "MLIC: Multi-reference entropy model for learned image compression," in *ACM MM*, 2023.
- [31] H. Li, S. Li, W. Dai, C. Li, J. Zou, and H. Xiong, "Frequency-aware transformer for learned image compression," in *ICLR*, 2024.
- [32] S.-Y. Qin, J. Wang, Y. Zhou, B. Chen, T. Luo, B. An, T. Dai, S.-T. Xia, and Y. Wang, "MambaVC: Learned visual compression with selective state spaces," *ArXiv*, vol. 2405.15413, 2024.
- [33] F. Zeng, H. Tang, Y. Shao, S. Chen, L. Shao, and Y. Wang, "MambaIC: State space models for high-performance learned image compression," in *CVPR*, 2025.
- [34] A. D. la Fuente, S. Singh, and J. Ballé, "Fourier basis density model," in *PCS*, 2024.
- [35] I. V. Bajić, "Rate-accuracy bounds in visual coding for machines," in *IEEE MIPR*, 2025.
- [36] A. de Andrade and I. V. Bajic, "Towards task-compatible compressible representations," in *ICME Workshops*, 2024.
- [37] A. Harell, Y. Foroutan, N. A. Ahuja, P. Datta, B. Kanzariya, V. S. Somayazulu, O. Tickoo, A. de Andrade, and I. V. Bajic, "Rate-distortion theory in coding for machines and its applications," *IEEE TPAMI*, 2025.
- [38] L. G. Valiant, "A theory of the learnable," *ACM*, 1984.
- [39] P. J. Liu, M. Saleh, E. Pot, B. Goodrich, R. Sepassi, L. Kaiser, and N. Shazeer, "Generating Wikipedia by summarizing long sequences," in *ICLR*, 2018.
- [40] A. Radford and K. Narasimhan, "Improving language understanding by generative pre-training," <https://openai.com/index/language-unsupervised>, 2018.
- [41] H. Touvron, L. Martin, K. R. Stone, P. Albert, A. Almahairi, Y. Babaei, N. Bay Bahshlykov, S. Batra, P. Bhargava, S. Bhosale, D. M. Bikel, L. Blecher, C. tian Cantón Ferrer, M. Chen, G. Cucurull, D. Esiobu, J. Fernandes, J. Fu, W. Fu, B. Fuller, C. Gao, V. Goswami, N. Goyal, A. S. Hartshorn, S. Hosseini, R. Hou, H. Inan, M. Kardas, V. Kerkez, M. Khabsa, I. M. Kloumann, A. Korenev, P. S. Koura, M.-A. Lachaux, T. Lavril, J. Lee, D. Liskovich, Y. Lu, Y. Mao, X. Martinet, T. Mihaylov, P. Mishra, I. Molybog, Y. Nie, A. Poulton, J. Reizenstein, R. Rungta, K. Saladi, A. Schelten, R. Silva, E. M. Smith, R. Subramanian, X. Tan, B. Tang, R. Taylor, A. Williams, J. X. Kuan, P. Xu, Z. Yan, I. Zarov, Y. Zhang, A. Fan, M. H. M. Kambadur, S. Narang, A. Rodriguez, R. Stojnic, S. Edunov, and T. Scialom, "Llama 2: Open foundation and fine-tuned chat models," *ArXiv*, vol. 2307.09288, 2023.
- [42] Y. Zhong, S. Liu, J. Chen, J. Hu, Y. Zhu, X. Liu, X. Jin, and H. Zhang, "DistServe: Disaggregating prefill and decoding for goodput-optimized large language model serving," in *USENIX OSDI*, 2024.
- [43] E. Agustsson and L. Theis, "Universally quantized neural compression," in *NeurIPS*, 2020.
- [44] L. Theis, W. Shi, A. Cunningham, and F. Huszár, "Lossy image compression with compressive autoencoders," in *ICLR*, 2017.
- [45] J. Ballé, V. Laparra, and E. P. Simoncelli, "End-to-end optimization of nonlinear transform codes for perceptual quality," in *PCS*, 2016.
- [46] A. Karpathy, "NanoGPT," <https://github.com/karpathy/nanoGPT>, 2022.
- [47] I. Solaiman, M. Brundage, J. Clark, A. Askell, A. Herbert-Voss, J. Wu, A. Radford, and J. Wang, "Release strategies and the social impacts of language models," *ArXiv*, vol. 1908.09203, 2019.
- [48] A. Gokaslan, V. Cohen, E. Pavlick, and S. Tellex, "OpenWebText Corpus," <https://Skylion007.github.io/OpenWebTextCorpus>, 2019.
- [49] G. Bjontegaard, "Calculation of average PSNR differences between RD-curves," *ITU-T SC16/Q6 VCEG-M33*, 2001.
- [50] D. Paperno, G. Kruszewski, A. Lazaridou, Q. N. Pham, R. Bernardi, S. Pezzelle, M. Baroni, G. Boleda, and R. Fernández, "The LAMBADA dataset: Word prediction requiring a broad discourse context," in *ACL*, 2016.
- [51] P. Deutsch, "DEFLATE compressed data format specification version 1.3," *RFC*, 1996.
- [52] Y. Collet and M. S. Kucherawy, "Zstandard compression and the application/zstd media type," *RFC*, 2018.
- [53] Y. Uralsky, "Accelerating load times for DirectX games and apps with GDeflate for DirectStorage," <https://developer.nvidia.com/blog/accelerating-load-times-for-directx-games-and-apps-with-gdeflate-for-directstorage>, 2022.
- [54] J. Duda, "Asymmetric numeral systems: entropy coding combining speed of huffman coding with compression rate of arithmetic coding," *ArXiv*, vol. 1311.2540, 2013.
- [55] J. D. Cavanaugh, "Protocol overhead in IP/ATM networks," in *Minnesota Supercomputer Center*, 1994.
- [56] S. Biderman, H. Schoelkopf, Q. G. Anthony, H. Bradley, K. O'Brien, E. Hallahan, M. A. Khan, S. Purohit, U. S. Prashanth, E. Raff *et al.*, "Pythia: A suite for analyzing large language models across training and scaling," in *ICML*, 2023.
- [57] A. Dosovitskiy, L. Beyer, A. Kolesnikov, D. Weissenborn, X. Zhai, T. Unterthiner, M. Dehghani, M. Minderer, G. Heigold, S. Gelly, J. Uszkoreit, and N. Houlsby, "An image is worth 16x16 words: Transformers for image recognition at scale," in *ICLR*, 2021.
- [58] K. He, X. Zhang, S. Ren, and J. Sun, "Deep residual learning for image recognition," in *CVPR*, 2016.
- [59] G. W. Stewart, "A Krylov-Schur algorithm for large eigenproblems," *SIAM JMAA*, 2002.
- [60] R. B. Lehoucq, D. C. Sorensen, and C. Yang, *ARPACK users' guide: solution of large-scale eigenvalue problems with implicitly restarted Arnoldi methods*. SIAM, 1998.
- [61] J. Nocedal and S. J. Wright, *Numerical optimization*. Springer, 2006.
- [62] C. R. Johnson and R. A. Horn, *Matrix analysis*. Cambridge university press Cambridge, 1985.
- [63] P. L. Bartlett, O. Bousquet, and S. Mendelson, "Localized Rademacher complexities," in *COLT*, 2002.
- [64] L. Newhouse, M. Csail, R. P. Hess, M. Bcs, F. L. Cesista, I. A. Zahorodnii, J. Bernstein, and P. Isola, "Training transformers with enforced lipschitz constants," *ArXiv*, vol. 2507.13338, 2025.
- [65] J.-B. Hiriart-Urruty and C. Lemaréchal, *Convex analysis and minimization algorithms II: Advanced theory and bundle methods*. Springer Berlin, Heidelberg, 1993.
- [66] B. C. Geiger and G. Kubin, "On the information loss in memoryless systems: The multivariate case," *ArXiv*, vol. 1109.4856, 2011.
- [67] S. Kakade and A. Tewari, "Lecture notes in Rademacher composition and linear prediction," 2008.

- [68] M. Ledoux and M. Talagrand, *Probability in Banach Spaces: Isoperimetry and Processes*. Springer Berlin Heidelberg, 2013.
- [69] P. L. Bartlett and S. Mendelson, "Rademacher and gaussian complexities: Risk bounds and structural results," *JMLR*, 2002.
- [70] I. Loshchilov and F. Hutter, "Decoupled weight decay regularization," in *ICLR*, 2019.
- [71] O. Russakovsky, J. Deng, H. Su, J. Krause, S. Satheesh, S. Ma, Z. Huang, A. Karpathy, A. Khosla, M. S. Bernstein, A. C. Berg, and L. Fei-Fei, "ImageNet large scale visual recognition challenge," *IJCV*, 2015.
- [72] TorchVision maintainers and contributors, "TorchVision: PyTorch's computer vision library," *GitHub repository*, 2016.
- [73] A. Subramaniam, B. Karsin, D. LaSalle, G. Thomas-Collignon, M. Nicely, M. Milakov, M. Fan, N. Sakharnykh, and O. Lopicque, "Lossless compression on the GPU," <https://developer.nvidia.com/nvcomp>, 2021.
- [74] worldlife123, "torch_ans," https://github.com/worldlife123/torch_ans, 2026.



Anderson de Andrade (S'22) received his M.Sc. in Applied Computing from the University of Toronto in 2015 and obtained a B.Eng. degree in Networks and Communications in 2007 from Universidad Tecnológica del Centro. He is currently an Engineering Science Ph.D. student at Simon Fraser University. His research interests include learned compression, information theory, and learning theory. He has published at major conferences, including ICLR, and EMNLP, and has been awarded the NSERC CGS-D scholarship.



Alon Harell (S'19) received the M.A.Sc. degree in electrical engineering from Simon Fraser University, Burnaby, BC, Canada in 2020 focusing on deep learning applications for non-intrusive load monitoring. Since 2020 Alon has been pursuing his PhD in engineering science at Simon Fraser University. His research interests include information theory as it applies to deep learning, coding for machines, and sports analytics. He has published at major conferences including ICASSP, ICM Multimedia, and AAAI, and has been awarded both NSERC

CGS-M and PGS-D scholarships.



Ivan V. Bajić (S'99–M'04–SM'11) is a Professor of Engineering Science and co-director of the Multimedia Lab at Simon Fraser University, Canada. His research interests include signal processing and machine learning with applications to multimedia signal processing, compression, and collaborative intelligence. His group's work has received the 2023 IEEE TCSVT Best Paper Award, conference paper awards at ICME 2012, ICIP 2019, MMSP 2022, and ISCAS 2023, and other recognitions (e.g., paper award finalist, top n%) at Asilomar, ICIP, ICME, and CVPR. He is the Past Chair of the IEEE Multimedia Signal Processing Technical Committee and currently serves as a Senior Area Editor of IEEE Signal Processing Letters.

Supplementary Material: Rate-Distortion Optimization for Transformer Inference

VI. S-I. THEORETICAL RESULTS AND PROOFS

A. The \mathcal{V} -entropy gap in terms of KL divergences

Lemma 1. Let $\mathcal{V} \subseteq \Omega$ be a predictive family according to [9], and Y and W two random variables with sample space \mathcal{Y} and \mathcal{W} respectively. Then:

$$G_{\mathcal{V}}(Y|W) = \inf_{g \in \mathcal{V}} \mathbb{E}_{\mathbf{w} \sim W} [\text{KL}(P_{Y|\mathbf{w}} \| g[\mathbf{w}])]. \quad (9)$$

Proof.

$$G_{\mathcal{V}}(Y|W) \triangleq |H_{\mathcal{V}}(Y|W) - H_{\Omega}(Y|W)| \quad (10)$$

$$= \left| \inf_{g \in \mathcal{V}} \mathbb{E}_{\mathbf{y}, \mathbf{w} \sim Y, W} [-\log g[\mathbf{w}](\mathbf{y})] - \inf_{\omega \in \Omega} \mathbb{E}_{\mathbf{y}, \mathbf{w} \sim Y, W} [-\log \omega[\mathbf{w}](\mathbf{y})] \right| \quad (11)$$

$$= \left| \inf_{g \in \mathcal{V}} \mathbb{E}_{\mathbf{y}, \mathbf{w} \sim Y, W} [-\log g[\mathbf{w}](\mathbf{y})] - \mathbb{E}_{\mathbf{y}, \mathbf{w} \sim Y, W} [-\log P_{Y|W}(\mathbf{y}|\mathbf{w})] \right| \quad (12)$$

$$= \inf_{g \in \mathcal{V}} \mathbb{E}_{\mathbf{y}, \mathbf{w} \sim Y, W} [-\log g[\mathbf{w}](\mathbf{y})] - \mathbb{E}_{\mathbf{y}, \mathbf{w} \sim Y, W} [-\log P_{Y|W}(\mathbf{y}|\mathbf{w})] \quad (13)$$

$$= \inf_{g \in \mathcal{V}} \mathbb{E}_{\mathbf{w} \sim W} \left[\mathbb{E}_{\mathbf{y} \sim Y|\mathbf{w}} \left[\log \frac{P_{Y|W}(\mathbf{y}|\mathbf{w})}{g[\mathbf{w}](\mathbf{y})} \right] \right] \quad (14)$$

$$= \inf_{g \in \mathcal{V}} \mathbb{E}_{\mathbf{w} \sim W} [\text{KL}(P_{Y|\mathbf{w}} \| g[\mathbf{w}])]. \quad (15)$$

Eq. 12 was obtained due to $\forall \mathbf{w} \in \mathcal{W}, P_{Y|\mathbf{w}} \in \Omega$ and $H(P_{Y|\mathbf{w}}, P_{Y|\mathbf{w}}) \leq H(P_{Y|\mathbf{w}}, \omega[\mathbf{w}])$. $H(\cdot, \cdot)$ is the cross-entropy measure. Eq. 13 was obtained due to $\mathcal{V} \subseteq \Omega$. \square

B. The rate term in the optimization objective as a bound of the \mathcal{V} -entropy gap

Theorem 1. Let \mathcal{V}_w be a predictive family of entropy models for the hyper-prior W , and $\mathcal{V}_{g_y} \subseteq \{\mathcal{W} \cup \{\emptyset\} \rightarrow \mathcal{N}(\mathcal{Y}; \Lambda)\}$ be a predictive family of conditional entropy models g_y for the target representation, where Λ is a set of all diagonal covariance matrices. Let $\mathcal{H}(\delta); \exists h \in \mathcal{H}(\delta) : W = (q \circ h)(Y)$ be a set of constrained hyper-prior functions such that $H_{\mathcal{V}_w}(W) \leq \delta, \delta \geq 0$. Defining a constrained predictive family $\bar{\mathcal{V}}_y = \mathcal{H}(\delta) \times \{q\} \times \mathcal{V}_{g_y}$, we have that:

$$G_{\bar{\mathcal{V}}_y}(Y|Y) = H_{\bar{\mathcal{V}}_y}(Y|Y) \leq \min \mathbb{E} [r_y(Y; W) + r_w(W)],$$

where the minimum is over the unconstrained predictive families $\mathcal{V}_y = \mathcal{H}(\infty) \times \{q\} \times \mathcal{V}_{g_y}$, and \mathcal{V}_w .

Proof.

$$G_{\bar{\mathcal{V}}_y}(Y|Y) = H_{\bar{\mathcal{V}}_y}(Y|Y) - H_{\Omega}(Y|Y) \quad (16)$$

$$= H_{\bar{\mathcal{V}}_y}(Y|Y) \quad (17)$$

$$\leq \min_{(h, q, g_y) \in \bar{\mathcal{V}}_y} \{ \mathbb{E}_{\mathbf{y} \sim Y} [-\log g_y[(q \circ h)(\mathbf{y})](\mathbf{y})] + \lambda_w (H_{\mathcal{V}_w}(W) - \delta) \} \quad (18)$$

$$\leq \min_{(h, q, g_y) \in \bar{\mathcal{V}}_y} \{ \mathbb{E}_{\mathbf{y} \sim Y} [-\log g_y[(q \circ h)(\mathbf{y})](\mathbf{y})] + \lambda_w H_{\mathcal{V}_w}(W) \} \quad (19)$$

$$\leq \min_{(h, q, g_y) \in \bar{\mathcal{V}}_y} \left\{ \mathbb{E}_{\mathbf{y} \sim Y} [-\log g_y[(q \circ h)(\mathbf{y})](\mathbf{y})] + \min_{g_w \in \mathcal{V}_w} \mathbb{E} [-\log g_w[\emptyset](\mathbf{W})] \right\} \quad (20)$$

$$\leq \min_{(h, q, g_y) \in \bar{\mathcal{V}}_y, g_w \in \mathcal{V}_w} \{ \mathbb{E}_{\mathbf{y} \sim Y} [-\log g_y[(q \circ h)(\mathbf{y})](\mathbf{y})] + \mathbb{E} [-\log g_w[\emptyset](\mathbf{W})] \} \quad (21)$$

$$= \min \mathbb{E} [r_y(Y; W) + r_w(W)]. \quad (22)$$

Eq. 17 uses $H_{\Omega}(Y|Y) = 0$. Eq. 18 uses the Lagrangian relaxation solution as a bound [65]. Eq. 20 uses $\lambda_w \leq 1$ since a higher rate cost for W could result in an undesirable situation in which no information is placed on W . \square

C. Lipschitz bound for the \mathcal{V} -entropy gap assuming side information as a function of a common ancestor

We assume that the target representation Y and the side information W originate from the same input X so that the functions generating them are invertible. Due to invertibility, both representations contain all information about the input and each other. We demonstrate that even in this unlikely situation for neural networks, the choice of input transformations can produce an increase in the \mathcal{V} -entropy gap independently of the choice of entropy model.

Before showing the main result of this section, we introduce the following lemma and its proof:

Lemma 2. Given $Y = f(X), W = h(X)$, where X is a continuous random variable, and f, h are bijective and Lipschitz continuous with constants L_f, L_h respectively, we have:

$$\mathbb{E}_{\mathbf{x} \sim X} \left[\log \frac{|J_{h(\mathbf{x})}|}{|J_{f(\mathbf{x})}|} \right] \leq D(L_h + L_{f^{-1}} - 2) \quad (23)$$

Proof.

$$\mathbb{E}_{\mathbf{x} \sim X} \left[\log \frac{|J_{h(\mathbf{x})}|}{|J_{f(\mathbf{x})}|} \right] = \mathbb{E}_{\mathbf{x} \sim X} \left[\log \frac{\left| \prod_{i=1}^D \lambda_i(J_{h(\mathbf{x})}) \right|}{\left| \prod_{i=1}^D \lambda_i(J_{f(\mathbf{x})}) \right|} \right] \quad (24)$$

$$= \mathbb{E}_{\mathbf{x} \sim X} \left[\sum_{i=1}^D \log |\lambda_i(J_{h(\mathbf{x})})| - \sum_{i=1}^D \log |\lambda_i(J_{f(\mathbf{x})})| \right] \quad (25)$$

$$\leq \mathbb{E}_{\mathbf{x} \sim X} \left[\sum_{i=1}^D \{ |\lambda_i(J_{h(\mathbf{x})})| - 1 \} - \sum_{i=1}^D \left\{ 1 - \frac{1}{|\lambda_i(J_{f(\mathbf{x})})|} \right\} \right] \quad (26)$$

$$= \mathbb{E}_{\mathbf{x} \sim X} \left[\sum_{i=1}^D |\lambda_i(J_{h(\mathbf{x})})| + \sum_{i=1}^D \frac{1}{|\lambda_i(J_{f(\mathbf{x})})|} \right] - 2D \quad (27)$$

$$= \mathbb{E}_{\mathbf{x} \sim X} \left[\|\boldsymbol{\lambda}(J_{h(\mathbf{x})})\|_1 + \|\boldsymbol{\lambda}(J_{f(\mathbf{x})}^{-1})\|_1 \right] - 2D \quad (28)$$

$$\leq \sqrt{D} \mathbb{E}_{\mathbf{x} \sim X} \left[\|\boldsymbol{\lambda}(J_{h(\mathbf{x})})\|_2 + \|\boldsymbol{\lambda}(J_{f(\mathbf{x})}^{-1})\|_2 \right] - 2D \quad (29)$$

$$= \sqrt{D} \mathbb{E}_{\mathbf{x} \sim X} \left[\|J_{h(\mathbf{x})}\|_{\text{F}} + \|J_{f(\mathbf{x})}^{-1}\|_{\text{F}} \right] - 2D \quad (30)$$

$$\leq D \mathbb{E}_{\mathbf{x} \sim X} \left[\|J_{h(\mathbf{x})}\|_2 + \|J_{f(\mathbf{x})}^{-1}\|_2 \right] - 2D \quad (31)$$

$$= D \mathbb{E}_{\mathbf{x} \sim X} \left[\|J_{h(\mathbf{x})}\|_2 + \|J_{f^{-1}(f(\mathbf{x}))}\|_2 \right] - 2D \quad (32)$$

$$\leq D(L_h + L_{f^{-1}} - 2). \quad (33)$$

Eq. 26 uses the logarithmic bounds $\log a \leq a - 1; \log a \geq 1 - 1/a$. Eq. 28 uses the fact that $\forall \lambda_i(A) \in \boldsymbol{\lambda}(A) \exists 1/\lambda_i(A) \in \boldsymbol{\lambda}(A^{-1})$. Eq. 29 uses the bound for the 1-norm $\|\mathbf{a}\|_1 \leq \sqrt{|\mathbf{a}|} \|\mathbf{a}\|_2$. Eq. 30 uses the bound for the 2-norm $\|\boldsymbol{\lambda}(A)\|_2 = \|A\|_{\text{F}}$. Eq. 31 uses the Frobenius norm bound $\|A\|_{\text{F}} \leq \sqrt{\text{rank}(A)} \|A\|_2$. Eq. 32 uses the relationship between Jacobian inverses $J_{f(\mathbf{x})}^{-1} = J_{f^{-1}(f(\mathbf{x}))}$. Finally, Eq. 33 uses the Lipschitz continuity assumption of f and h and the Jacobian 2-norm bound $\|J_{f(\mathbf{x})}\|_2 \leq L_f \forall \mathbf{x} \in \mathbb{R}^D$. \square

Theorem 5. Let $\mathcal{V} \subseteq \Omega$ be a predictive family according to [9], $Y = f(X), W = h(X)$, where X is a continuous random variable, and f, h are bijective and Lipschitz continuous with constants L_f, L_h respectively, and \mathcal{Y}, \mathcal{W} are the sample spaces of Y, W respectively. Then:

$$G_{\mathcal{V}}(Y|W) \leq \inf_{g \in \mathcal{V}} \mathbb{E}[-\log g[W](Y)] + D(L_h + L_{f^{-1}} - 2),$$

where $L_{f^{-1}}$ is the Lipschitz constant of the inverse of f .

Proof. Since random variables Y and W share a common ancestor X , using the change of variables, their probabilities are related by:

$$P_Y(f(\mathbf{x})) = P_W(h(\mathbf{x})) \frac{|J_{h(\mathbf{x})}|}{|J_{f(\mathbf{x})}|}, \quad (34)$$

where $|J_{v(\mathbf{x})}|$ is the absolute Jacobian determinant of $v(\mathbf{x})$. Thus:

$$G_{\mathcal{V}}(Y|W) = \inf_{g \in \mathcal{V}} \mathbb{E}_{\mathbf{w} \sim W} \left[\mathbb{E}_{\mathbf{y} \sim Y|\mathbf{w}} \left[\log \frac{P_{Y|W}(\mathbf{y}|\mathbf{w})}{g[\mathbf{w}](\mathbf{y})} \right] \right] \quad (35)$$

$$= \inf_{g \in \mathcal{V}} \mathbb{E}_{\mathbf{w} \sim W} \left[\mathbb{E}_{\mathbf{y} \sim Y|\mathbf{w}} \left[\log \frac{P_{W|Y}(\mathbf{w}|\mathbf{y})P_Y(\mathbf{y})}{g[\mathbf{w}](\mathbf{y})P_W(\mathbf{w})} \right] \right] \quad (36)$$

$$= \inf_{g \in \mathcal{V}} \mathbb{E}_{\mathbf{w}, \mathbf{y} \sim W, Y} \left[\log \frac{P_{W|Y}(\mathbf{w}|\mathbf{y})}{g[\mathbf{w}](\mathbf{y})} \right] + \mathbb{E}_{\mathbf{x} \sim X} \left[\mathbb{E}_{\mathbf{y} \sim Y|h(\mathbf{x})} \left[\log \frac{P_Y(\mathbf{y})}{P_W(h(\mathbf{x}))} \right] \right] \quad (37)$$

$$= \inf_{g \in \mathcal{V}} \mathbb{E}_{\mathbf{w}, \mathbf{y} \sim W, Y} \left[\log \frac{P_{W|Y}(\mathbf{w}|\mathbf{y})}{g[\mathbf{w}](\mathbf{y})} \right] + \mathbb{E}_{\mathbf{x} \sim X} \left[\log \frac{|J_h(\mathbf{x})|}{|J_f(\mathbf{x})|} \right] \quad (38)$$

$$\leq \inf_{g \in \mathcal{V}} \mathbb{E}_{\mathbf{w}, \mathbf{y} \sim W, Y} \left[\log \frac{P_{W|Y}(\mathbf{w}|\mathbf{y})}{g[\mathbf{w}](\mathbf{y})} \right] + D(L_h + L_{f^{-1}} - 2) \quad (39)$$

$$= \inf_{g \in \mathcal{V}} \left\{ \mathbb{E}_{\mathbf{w}, \mathbf{y} \sim W, Y} [\log P_{W|Y}(\mathbf{w}|\mathbf{y})] + \mathbb{E}_{\mathbf{w}, \mathbf{y} \sim W, Y} [-\log g[\mathbf{w}](\mathbf{y})] \right\} + D(L_h + L_{f^{-1}} - 2) \quad (40)$$

$$= \inf_{g \in \mathcal{V}} \mathbb{E}_{\mathbf{w}, \mathbf{y} \sim W, Y} [-\log g[\mathbf{w}](\mathbf{y})] + D(L_h + L_{f^{-1}} - 2). \quad (41)$$

Eq. 36 uses Bayes' theorem. Eq. 38 uses Eq. 34. Eq. 39 uses Lemma 2. Eq. 41 is due to $P_{W|Y}$ being degenerate since f and h are bijective. \square

We see that the \mathcal{V} -entropy increases as h expands and f contracts. The first term is the conditional cross-entropy between the true distribution $P_{Y,W}$ and the best entropy model. The second term cancels when f and h are identity functions.

D. Lipschitz bound for the \mathcal{V} -entropy gap assuming fixed side information as a function of the target representation

This formulation offers an alternative view in cases where the side information is considered fixed, such that the hyper-prior analysis transform h is not part of the predictive family. The second term cancels when h becomes the identity function.

Theorem 6. Let $\mathcal{V} \subseteq \Omega$ be a predictive family according to [9], $Y = f(X)$, $W = h(Y)$, where X is a continuous random variable, f and h are bijective, h is Lipschitz continuous with constant L_h , and \mathcal{Y} , \mathcal{W} are the sample spaces of Y , W respectively. Then:

$$G_{\mathcal{V}}(Y|W) \leq \inf_{g \in \mathcal{V}} \mathbb{E} [-\log g[W](Y)] + D(L_h - 1). \quad (42)$$

Proof. Following the proof for Lemma 2 closely, we arrive at:

$$\mathbb{E}_{\mathbf{x} \sim X} \left[\log \frac{|J_{(h \circ f)(\mathbf{x})}|}{|J_f(\mathbf{x})|} \right] = \mathbb{E}_{\mathbf{x} \sim X} \left[\log \frac{|J_h(f(\mathbf{x}))J_f(\mathbf{x})|}{|J_f(\mathbf{x})|} \right] \quad (43)$$

$$= \mathbb{E}_{\mathbf{x} \sim X} [\log |J_h(f(\mathbf{x}))|] \quad (44)$$

$$= \mathbb{E}_{\mathbf{x} \sim X} \left[\log \left| \prod_{i=1}^D \lambda_i (J_h(f(\mathbf{x}))) \right| \right] \quad (45)$$

$$\leq \mathbb{E}_{\mathbf{x} \sim X} \left[\sum_{i=1}^D |\lambda_i (J_h(f(\mathbf{x})))| \right] - D \quad (46)$$

$$\leq D \mathbb{E}_{\mathbf{x} \sim X} [\|J_h(f(\mathbf{x}))\|_2] - D \quad (47)$$

$$\leq D(L_h - 1). \quad (48)$$

Plugging this result into Eq. 38 and changing variables with respect to X reaches the result. \square

E. Bounds for \mathcal{V} -entropy

Theorem 2. Let $\mathcal{V} \subseteq \Omega$ be a predictive family according to [9], and $Y = q(Y'; \Delta)$ the quantization of a continuous random variable with $\text{cov}(Y') = \Sigma$, where Δ is the maximum quantization step. Then, with $D = |Y| = T \times E$, we have:

$$H_{\mathcal{V}}(Y|W) \leq 1/2 \log \det \Sigma + D/2 \log (2\pi e) + G_{\mathcal{V}}(Y|W) - \log \Delta \quad \text{as } \Delta \rightarrow 0.$$

Proof. Starting from Eq. 3, we have:

$$H_{\mathcal{V}}(Y|W) = \inf_{g \in \mathcal{V}} \mathbb{E}_{\mathbf{y}, \mathbf{w} \sim Y, W} [-\log g[\mathbf{w}](\mathbf{y})] \quad (49)$$

$$= \inf_{g \in \mathcal{V}} \mathbb{E}_{\mathbf{y}, \mathbf{w} \sim Y, W} \left[\log \frac{P_{Y|W}(\mathbf{y}|\mathbf{w})}{g[\mathbf{w}](\mathbf{y})P_{Y|W}(\mathbf{y}|\mathbf{w})} \right] \quad (50)$$

$$= H(Y|W) + \inf_{g \in \mathcal{V}} \mathbb{E}_{\mathbf{y}, \mathbf{w} \sim Y, W} \left[\log \frac{P_{Y|W}(\mathbf{y}|\mathbf{w})}{g[\mathbf{w}](\mathbf{y})} \right] \quad (51)$$

$$= H(Y|W) + G_{\mathcal{V}}(Y|W) \quad (52)$$

$$\leq H(Y) + G_{\mathcal{V}}(Y|W) \quad (53)$$

$$= h(Y') + G_{\mathcal{V}}(Y|W) - \log \Delta \quad \text{as } \Delta \rightarrow 0 \quad (54)$$

$$\leq 1/2 \log \det \Sigma + D/2 \log(2\pi e) + G_{\mathcal{V}}(Y|W) - \log \Delta \quad \text{as } \Delta \rightarrow 0. \quad (55)$$

Eq. 52 uses Lemma 1. Eq. 53 uses $H(Y) \leq H(Y|\cdot)$ for any random variable Y [7]. Eq. 54 uses $H(Y) \rightarrow h(Y') - \log \Delta$ as $\Delta \rightarrow 0$ [7]. Eq. 55 uses the differential entropy of a Gaussian distribution with covariance Σ as an upper-bound on the differential entropy of any random variable with the same covariance [7]. \square

Theorem 3. Let $\mathcal{V} \subseteq \Omega$ be a predictive family according to [9], and $Y = q(Y'; \Delta)$ the quantization of a L_f -Lipschitz function of a continuous random variable X such that $Y' = f(X)$, with $\text{cov}(Y') = \Sigma$, where Δ is the maximum quantization step. Then, with $D = |Y| = T \times E$, we have:

$$H_{\mathcal{V}}(Y|W) \leq h(X) + D(L_f - 1) + G_{\mathcal{V}}(Y|W) - \log \Delta \quad \text{as } \Delta \rightarrow 0.$$

Proof. Starting from Eq. 54, we have:

$$H_{\mathcal{V}}(Y|W) \leq h(Y') + G_{\mathcal{V}}(Y|W) - \log \Delta \quad \text{as } \Delta \rightarrow 0 \quad (56)$$

$$\leq h(X) + \mathbb{E} [\log |J_{f(X)}|] + G_{\mathcal{V}}(Y|W) - \log \Delta \quad \text{as } \Delta \rightarrow 0 \quad (57)$$

$$\leq h(X) + D(L_f - 1) + G_{\mathcal{V}}(Y|W) - \log \Delta \quad \text{as } \Delta \rightarrow 0. \quad (58)$$

Eq. 57 uses an well-known upper-bound on the entropy of a function of a continuous random variable [66]. Eq. 58 uses the same derivation that produces Eq. 48 from Eq. 44. \square

F. Generalization bound for the \mathcal{V} -entropy gap

Theorem 4. Let $\mathcal{V} \subseteq \Omega$ be a predictive family according to [9], Y and W random variables with sample spaces \mathcal{Y} and \mathcal{W} , respectively, with $\mathcal{D} = \{(\mathbf{y}_i, \mathbf{w}_i)\}_{i=1}^N \sim Y, W$ as a set of samples. Assume that $\forall g \in \mathcal{V}, \mathbf{y} \in \mathcal{Y}, \mathbf{w} \in \mathcal{W}, \log g[\mathbf{w}](\mathbf{y}) \in [-B, B], \log P_{Y|W}(\mathbf{y}|\mathbf{w}) \in [-B, B]$, and that the Lipschitz constant of $P_{Y|\mathbf{w}} \forall \mathbf{w} \in \mathcal{W}$ is governed by the Lipschitz constant of a multivariate normal distribution with covariance matrix αI , such that $\alpha \leq \exp(2BD^{-1})(2\pi)^{-1}$. Then, $\forall \delta \in (0, 1)$, with probability at least $1 - \delta$, we have:

$$R_{\mathcal{V}, \mathcal{D}}(Y|W) \leq 2 \left[(\text{Lip}(\mathcal{V}_r) + \beta) \text{Rad}(\mathcal{D}) + B \sqrt{2/N \log 1/\delta} \right],$$

where $\text{Rad}(\mathcal{D})$ is the Rademacher complexity of the concatenated samples in the dataset \mathcal{D} , $\text{Lip}(\mathcal{V}_r)$ is the maximum Lipschitz constant in $\mathcal{V}_r = \{v|v(\mathbf{w}, \mathbf{y}) = \log g[\mathbf{w}](\mathbf{y}), g \in \mathcal{V}\}$, and:

$$\beta \triangleq \alpha^{-1/2} [2B - D \log(2\pi\alpha)]^{1/2}.$$

Proof. The assumption that $\log P_{Y|w} \in [-B, B]$ implies that:

$$-1/2(\mathbf{y} - \boldsymbol{\mu})^\top (\alpha I)^{-1} (\mathbf{y} - \boldsymbol{\mu}) - D/2 \log(2\pi\alpha) \geq -B \quad (59)$$

$$\implies \|\mathbf{y} - \boldsymbol{\mu}\|_2 \leq \alpha^{1/2} [2B - D \log(2\pi\alpha)]^{1/2}, \quad (60)$$

where, to keep the right-hand-side positive as required by the norm, implies:

$$2B - D \log(2\pi\alpha) \geq 0 \implies \alpha \leq \exp(2BD^{-1})(2\pi)^{-1}. \quad (61)$$

The Lipschitz constant of $\log P_{Y|w}$ under the assumed constraint is upper-bounded as:

$$\text{Lip}(\log P_{Y|w}) = \sup_{\mathbf{y} \in \mathbb{R}^D} \|\nabla \log \mathcal{N}(\mathbf{y}; \boldsymbol{\mu}, \alpha I)\|_\infty \quad (62)$$

$$= \alpha^{-1} \sup_{\mathbf{y} \in \mathbb{R}^D} \|\mathbf{y} - \boldsymbol{\mu}\|_\infty \quad (63)$$

$$\leq \alpha^{-1} \sup_{\mathbf{y} \in \mathbb{R}^D} \|\mathbf{y} - \boldsymbol{\mu}\|_2 \quad (64)$$

$$\leq \alpha^{-1/2} [2B - D \log(2\pi\alpha)]^{1/2} \quad (65)$$

$$\triangleq \beta. \quad (66)$$

Eq. 65 is obtained by plugging in Eq. 60. Finally, with $\hat{g} = \arg \min_{g \in \mathcal{V}} \sum_{(\mathbf{y}, \mathbf{w}) \in \mathcal{D}} -\log g[\mathbf{w}](\mathbf{y})$, we derive:

$$R_{\mathcal{V}, \mathcal{D}}(Y|W) \triangleq \left| G_{\mathcal{V}}(Y|W) - \inf_{g \in \mathcal{V}} \frac{1}{N} \sum_{(\mathbf{y}, \mathbf{w}) \in \mathcal{D}} \log \frac{P_{Y|W}(\mathbf{y}|\mathbf{w})}{g[\mathbf{w}](\mathbf{y})} \right| \quad (67)$$

$$= \left| H_{\mathcal{V}}(Y|W) - H_{\Omega}(Y|W) - \frac{1}{N} \sum_{(\mathbf{y}, \mathbf{w}) \in \mathcal{D}} \log \frac{P_{Y|W}(\mathbf{y}|\mathbf{w})}{\hat{g}[\mathbf{w}](\mathbf{y})} \right| \quad (68)$$

$$\leq \left| H_{\mathcal{V}}(Y|W) - \frac{1}{N} \sum_{(\mathbf{y}, \mathbf{w}) \in \mathcal{D}} -\log \hat{g}[\mathbf{w}](\mathbf{y}) \right| + \left| \frac{1}{N} \sum_{(\mathbf{y}, \mathbf{w}) \in \mathcal{D}} -\log P_{Y|W}(\mathbf{y}|\mathbf{w}) - H_{\Omega}(Y|W) \right| \quad (69)$$

$$\leq 2 \text{Rad}(\mathcal{V}_r \circ \mathcal{D}) + 2 \text{Rad}(\log P_{Y|W} \circ \mathcal{D}) + 2B \sqrt{2/N \log 1/\delta} \quad (70)$$

$$\leq 2 \text{Lip}(\mathcal{V}_r) \text{Rad}(\mathcal{D}) + 2 \text{Lip}(\log P_{Y|W}) \text{Rad}(\mathcal{D}) + 2B \sqrt{2/N \log 1/\delta} \quad (71)$$

$$\leq 2 \left[\text{Lip}(\mathcal{V}_r) \text{Rad}(\mathcal{D}) + \beta \text{Rad}(\mathcal{D}) + B \sqrt{2/N \log 1/\delta} \right] \quad (72)$$

$$= 2 \left[(\text{Lip}(\mathcal{V}_r) + \beta) \text{Rad}(\mathcal{D}) + B \sqrt{2/N \log 1/\delta} \right]. \quad (73)$$

Eq. 69 uses the triangle inequality. Eq. 70 uses Lemma 3 in [9] on each of the two terms, where the predictive family for the second term has been reduced to $\{P_{Y|W}\}$. Eq. 71 uses the Kakade & Tewari Lemma [67] based on Talagrand's contraction principle [68], [69]. It states that if all vectors in a set A are operated by a Lipschitz function, then $\text{Rad}(A)$ is at most multiplied by the Lipschitz constant of the function. Eq. 72 uses Eq. 66. Similarly to $\text{Lip}(\mathcal{V}_r)$, $\text{Lip}(\log P_{Y|W})$ corresponds to the largest Lipschitz constant in $\{\log P_{Y|w}, w \in \mathcal{W}\}$. \square

G. Mathematical notation

Table I compiles the most relevant mathematical notation used in this work.

VII. S-II. ADDITIONAL RESULTS AND DETAILS

A. Entropy model definitions

Let $\mathcal{F}(\mathbb{R})$ be the set of all *cumulative density functions* (CDFs), and $\Theta = \{\boldsymbol{\theta}_1, \dots, \boldsymbol{\theta}_C\}$ be a set of parameter vectors for each embedding dimension of W . A zero-context learnable entropy model for the hyper-prior $g_w : \Theta \rightarrow \mathcal{F}(\mathbb{R})$ takes a parameter vector $\boldsymbol{\theta}_j; j = \{1, \dots, C\}$ to generate a CDF for any element in the j -th embedding dimension of W . The rate of a hyper-prior $w \sim W$ is the fully-factorized negative log-likelihood of a unit interval centered around \mathbf{w} :

$$r_w(\mathbf{w}) = - \sum_{i=1}^T \sum_{j=1}^C \log \left[g_w[\boldsymbol{\theta}_j](w_{i,j} + 1/2) - g_w[\boldsymbol{\theta}_j](w_{i,j} - 1/2) \right]. \quad (74)$$

Assuming a conditionally independent distribution for Y given W , the rate for $\mathbf{y} \sim Y$ is given by the negative log-likelihood of a unit interval centered around \mathbf{y} :

$$r_y(\mathbf{y}; \mathbf{w}) = - \sum_{i=1}^{T \times E} \log \left[\Phi(y_i + 1/2; g_\mu(\mathbf{w})_i, g_\sigma(\mathbf{w})_i) - \Phi(y_i - 1/2; g_\mu(\mathbf{w})_i, g_\sigma(\mathbf{w})_i) \right], \quad (75)$$

where $g_\mu : \mathcal{W} \rightarrow \mathbb{R}^{T \times E}$ and $g_\sigma : \mathcal{W} \rightarrow \mathbb{R}_+^{T \times E}$ correspond to the means and variances, respectively, produced by the entropy model g_y , Φ is the normal CDF, and i indexes the elements in the tensors.

TABLE I
NOTATION REFERENCE

Notation	Definition
$\mathbf{a} \sim A$	Rademacher random variable with sample space $\{-1, 1\}^N$
\mathcal{A}	M samples of A : $\mathcal{A} = \{\mathbf{a}_i\}_{i=1}^M \sim A$
B	Bound such that $\log g[\mathbf{w}](\mathbf{y}), \log P_{Y W}(\mathbf{y} \mathbf{w}) \in [-B, B]$
C	Embedding size of the side information: $W \in \mathbb{R}^{T \times C}$
D	Number of elements in Y such that $D = Y = T \times E$
\mathcal{D}	N data samples: $\mathcal{D} = \{\mathbf{y}_i\}_{i=1}^N \sim Y$
$d(\hat{\mathbf{z}}, \mathbf{z})$	Task loss function or distortion function
E	Embedding size of the target representation: $Y \in \mathbb{R}^{T \times E}$
$f_{1,S}(X)$	Function producing the target representation Y
$f_{S+1,L}(Y)$	Second split/module of the neural network, without header layers
$f_l(\cdot)$	Transformer block: $\{f_l : \mathbb{R}^{T \times E} \rightarrow \mathbb{R}^{T \times E}\}_{l=1}^L$
$G_{\mathcal{V}}(\cdot \cdot)$	The \mathcal{V} -entropy gap, Definition 1
$g_{\mu}(W)$	Means produced by $g_y, g_{\mu} : \mathcal{W} \rightarrow \mathbb{R}^{T \times E}$
$g_{\sigma}(W)$	Variances produced by $g_y, g_{\sigma} : \mathcal{W} \rightarrow \mathbb{R}^{T \times E}$
$g_y(W)$	Entropy model for the target representation $g_y : \mathcal{W} \rightarrow \mathcal{N}(\mathcal{Y})$
$g_w(w_{i,j}; \theta_j)$	Entropy model for the hyper-prior $g_w : \mathbb{R} \rightarrow [0, 1]$
$H_{\mathcal{V}}(\cdot \cdot)$	Conditional \mathcal{V} -entropy, Eq. 3
$H(\cdot)$	Shannon's entropy
$H(\cdot, \cdot)$	Cross-entropy
$h(Y)$	Hyper-prior model $h : \mathcal{Y} \rightarrow \mathbb{R}^{T \times C}$
I	Identity matrix
$J_r(\mathbf{y})$	Jacobian matrix of function v evaluated at \mathbf{y}
$\text{KL}(\cdot \cdot)$	Kullback–Leibler divergence
L	Number of transformer blocks in a transformer-based neural network
$\mathcal{L}(Y, W, \hat{Z}, Z)$	Proposed loss function, Eq. 7
M	Number of samples from A : $ \mathcal{A} $
$\mathcal{N}, \mathcal{N}(\mathcal{Y})$	Normal PDF, or the set of all normal PDFs on \mathcal{Y}
N	Dataset size $ \mathcal{D} $
$q(\cdot)$	Quantization function
$R_{\mathcal{V}, \mathcal{D}}(\cdot \cdot)$	Generalization error of the \mathcal{V} -entropy gap, Definition 2
$r_y(\mathbf{y}; \mathbf{w})$	Rate function for the target representation, Eq. 75
$r_w(\mathbf{w})$	Rate function for the side-information, Eq. 74
S	Split point $S \in \{1, \dots, L\}$
T	Target representation context size: $Y \in \mathbb{R}^{T \times E}$
$t(\cdot)$	$t : \mathbb{R}^{T \times E} \rightarrow \mathcal{Z}$, head module producing predictions \hat{Z} for target Z
\mathcal{V}	Predictive family [9]
\mathcal{V}_r	Set of log probability functions of \mathcal{V} : $\{v v(\mathbf{w}, \mathbf{y}) = \log g[\mathbf{w}](\mathbf{y}), g \in \mathcal{V}\}$
$\mathbf{w} \sim W, \mathbf{w} \in \mathcal{W}$	Side information with sample space $\mathcal{W} \subseteq \mathbb{R}^{T \times C}$
$\mathbf{x} \sim X, \mathbf{x} \in \mathcal{X}$	Input with $\mathcal{X} \subseteq \mathbb{R}^{T \times E}$
$\mathbf{y} \sim Y, \mathbf{y} \in \mathcal{Y}$	Target representation with $\mathcal{Y} \subseteq \mathbb{R}^{T \times C}$
$\mathbf{z} \sim Z, \mathbf{z} \in \mathcal{Z}$	Task target
$\hat{\mathbf{z}} \sim \hat{Z}, \hat{\mathbf{z}} \in \mathcal{Z}$	Model prediction
α	Variance factor in Theorem 4, where $\alpha \leq \exp(2BD^{-1})(2\pi)^{-1}$
Δ	Quantization step
Θ	Parameters of the hyper-prior entropy model: $\Theta = \{\theta_j, \dots, \theta_C\}$
Λ	The set of all diagonal covariance matrices
λ	Rate-distortion trade-off parameter
Φ	Normal CDF
Ω	Set of all probability functions over \mathcal{Y} such that $\Omega = \{W \cup \{\emptyset\} \rightarrow \mathcal{P}(\mathcal{Y})\}$

B. Result breakdown

Tables II, III, and IV provide the task performances achieved for the models and the corresponding tasks evaluated in Section IV. Confidence intervals for the estimates of the Rademacher complexity of the analysis transform, the covariance determinant of the target representation, and the Lipschitz constant of the entropy model are provided at a confidence level of 99%. Different randomly-selected subsets of the validation dataset are used for each sample. Any source of randomness used in the computation of the estimates is also different between samples. The underlying models are the same across samples.

C. Experimental settings and resource details

The text is processed using the TikToken GPT-2 tokenizer [47] and each sample has $T = 1024$ tokens, where different documents in the sequence are separated by a special token. Following [46], we use a linear warmup followed by a cosine learning rate schedule for AdamW [70], with coefficients $\beta_1 = 0.9, \beta_2 = 0.95$, and a weight decay of 0.1 placed on the two-dimensional parameter tensors of the language model. Using gradient accumulation, each optimization step uses 480 samples.

TABLE II
GPT-2 RATE-DISTORTION PERFORMANCE

Model	Split Pt.	λ	Hyper-Prior BPT	Total BPT	Perplexity	LAMBADA
Deep Factorized	3	0.001	39.73	249.48	20.74	0.2610
Deep Factorized	3	0.025	39.04	196.22	21.20	0.2558
Deep Factorized	3	0.075	33.59	153.23	21.69	0.2513
Deep Factorized	3	0.010	32.61	147.98	21.91	0.2414
Deep Factorized	6	0.001	45.55	355.93	20.89	0.2824
Deep Factorized	6	0.025	40.48	273.06	21.25	0.2723
Deep Factorized	6	0.075	36.31	214.98	22.69	0.2391
Deep Factorized	6	0.010	35.06	207.36	22.88	0.2389
Deep Factorized	9	0.001	52.71	492.08	21.61	0.2649
Deep Factorized	9	0.025	47.01	388.11	22.80	0.2503
Deep Factorized	9	0.075	40.53	288.44	24.59	0.2305
Deep Factorized	9	0.010	39.03	268.34	25.12	0.2245
Fourier	6	0.001	249.18	541.67	21.15	0.2946
Fourier	6	0.025	248.14	464.49	21.70	0.2800
Fourier	6	0.075	309.20	434.07	24.03	0.2212
Fourier	6	0.010	302.62	422.32	24.19	0.2069
Direct-Access	6	0.001	32.89	263.62	22.43	0.2663
Direct-Access	6	0.025	29.91	215.04	22.91	0.2554
Direct-Access	6	0.075	30.47	165.94	25.22	0.2296
Direct-Access	6	0.010	30.24	160.16	26.24	0.2084
Uncompressed	Any	–	–	12,288	20.71	0.2961

TABLE III
SPLIT POINT RATE-DISTORTION PERFORMANCE FOR LANGUAGE MODELS

Model	Split Pt.	λ	BPT	Perplexity	Rad(\mathcal{D})	log Lip(v)	$1/2D \log \text{Cov}(Y) $
GPT-2	3	0.010	148.7	19.10	1.18 ± 0.007	6.62 ± 0.097	4.57 ± 0.002
GPT-2	6	0.001	355.9	20.89	5.27 ± 0.052	4.21 ± 0.036	4.90 ± 0.002
GPT-2	9	0.001	492.1	21.61	13.53 ± 0.100	5.04 ± 0.107	5.35 ± 0.002
Pythia	3	0.001	371.5	21.36	9.95 ± 0.045	5.03 ± 0.046	5.17 ± 0.001
Pythia	6	0.001	451.9	21.99	12.12 ± 0.048	5.78 ± 0.044	5.26 ± 0.002
Pythia	8	0.001	513.6	22.39	14.39 ± 0.108	5.42 ± 0.033	5.26 ± 0.002

TABLE IV
SPLIT POINT RATE-DISTORTION PERFORMANCE FOR IMAGE CLASSIFICATION

Model	Split Pt.	λ	BPP	Accuracy	Rad(\mathcal{D})	log Lip(v)	$1/2D \log \text{Cov}(Y) $
ViT	3	0.01	2.35	0.79	0.12 ± 0.000	4.20 ± 0.011	3.99 ± 0.002
ViT	6	0.01	3.27	0.79	0.31 ± 0.001	4.16 ± 0.003	4.35 ± 0.003
ViT	9	0.01	5.15	0.79	0.56 ± 0.002	2.47 ± 0.006	5.53 ± 0.002
ResNet	3	0.01	4.75	0.68	1.87 ± 0.014	4.13 ± 0.008	5.93 ± 0.002
ResNet	7	0.01	2.65	0.67	1.12 ± 0.004	4.14 ± 0.009	5.76 ± 0.001
ResNet	13	0.01	1.20	0.67	1.03 ± 0.004	4.02 ± 0.018	5.38 ± 0.001

For convenience, all rate values reported correspond to estimates from the model. We noticed no change in distortion and less than 1% increase in rate when using the arithmetic coder, which could be mitigated with a small sacrifice in speed.

All models were trained on a single NVIDIA A40 GPU. During training, models required at most 20 GB of VRAM. All models were trained with bfloat16 precision except for the ones using the ResNet architecture. The estimates of Rademacher complexities, Lipschitz constants, and covariance determinants were computed using a single NVIDIA A40 GPU, on less than 5 GB of VRAM, taking at most 1 hour per measure and model. An estimate of 320 GPU hours were spent on preliminary experiments.

We use the OpenWebText split provided in [48]. The dataset is provided under the CC0 license. All results pertaining this dataset are reported on the validation set. The OpenWebText is treated as a contiguous text file and a sample is a random window of text with a context size of 1,024. An epoch is considered to be 1,000 gradient descent steps of 480,000 random samples. The validation set consists of 48,000 random samples.

The ImageNet-1k [71] is under a custom non-commercial license. Tasks trained on the dataset use the original splits. Each epoch trains on a subset of 100,000 random samples from the training set. All pertaining results are reported on the validation set. Random augmentations such as shearing, translation, rotation, and color jittering are applied to the samples, and MixUp

TABLE V
HYPER-PARAMETER SETTINGS

Parameter	GPT-2	Pythia	ViT	ResNet
Precision	bfloat16	bfloat16	bfloat16	float32
Target representation dimensionality (E)	768	768	768	768
Side information dimensionality (C)	24	24	24	24
Target representation context size (T)	1,024	1,024	49	49
Side information density parameters ($ \theta_j $)	118	118	118	118
Distortion function	cross-entropy	cross-entropy	cross-entropy	cross-entropy
Tokenizer	GPT-2	GPT-2	—	—
Label smoothing	—	—	0.11	0
MixUp coefficient	—	—	0.2	0.2
CutMix coefficient	—	—	1	1
Random augmentations	—	—	2	2
Augmentation magnitude	—	—	9	9
Batch size	12	12	16	16
Accumulated gradient batches	40	40	40	40
Optimizer	AdamW	AdamW	AdamW	AdamW
Optimizer parameters	(0.9, 0.95)	(0.9, 0.95)	(0.9, 0.95)	(0.9, 0.95)
Maximum learning rate	0.0006	0.0006	0.0006	0.0006
Minimum learning rate	0.00006	0.00006	0.00006	0.00006
Weight decay	0.1	0.1	0.3	0.001
Patience	5	5	5	5
Gradient norm clipping	1	1	1	1
Warm up function	linear	linear	linear	linear
Warm up steps	2,000	2,000	2,000	2,000
Schedule function	cosine	cosine	cosine	cosine
Maximum steps	600,000	600,000	600,000	600,000

and CutMix transformations are applied to a batch of size 16.

To produce the rate-distortion curves for the GPT-2 language models, a model is first trained from scratch with $\lambda = 0.0001$ for 50 epochs, or until no improvement has been achieved for more than 5 epochs. This takes around 120 hours. Finally, training is restarted for each $\lambda \in \{0.001, 0.0025, 0.0075, 0.01\}$ from the weights initially obtained. This training is done for around 25 epochs, or until no improvement has been attained for more than 5 epochs. This process usually takes 48 hours. For higher values of λ , the loss can diverge during training. In such cases, the maximum learning rate is set to 0.0001 and training is restarted from the checkpoint achieving the lowest loss.

For the Pythia language models, we use $\lambda = 0.001$. ViT and ResNet use $\lambda = 0.01$ on all experiments. The rate used as a loss term for the language models is computed in terms of bits-per-token (BPT), whereas the image classifiers use bits-per-pixel (BPP). The training of the Pythia language models starts from the weights provided in [56], under the Apache License, version 2.0. The ViT and ResNet methods use the weights provided in [72], under the BSD 3-Clause license.

Additional hyper-parameters are reported on Table V.

D. Bitrate and time comparisons

Deflate uses the LZ77 dictionary-matching compression algorithm and Huffman coding. It is used in the ZIP and PNG file formats. Zstandard combines LZ77 with a large search window and a fast entropy coder. It uses Huffman coding alongside finite-state entropy (FSE), a variant of a tabled asymmetric numeral system (tANS) [54].

We compare results on the same 1,000 random samples from the OpenWebText validation set. For the GPU benchmarks, we use the NVIDIA nvCOMP [73] GPU implementations of GDeflate and Zstandard. For the CPU benchmarks, we use the Python built-in version of Deflate, which is implemented using bindings to the *zlib* C library. For Zstandard, we use the *zstd* Python package, which also uses C bindings to the official implementation. The proposed method uses an implementation of a range asymmetric numeral system (rANS) coder called *torch_ans* [74].

We run the coding of each token in parallel from a batch of 10 samples with a context size of $T = 1024$. All benchmarks ran on a NVIDIA H100 SXM5 GPU with 16,896 cores, and 8 cores of an AMD EPYC 9454 CPU.

E. Comparative methods for the analysis of the rate-distortion performance and the split point

The language modeling tasks use the same dataset and settings as discussed in Section IV-B. The image classification tasks use ImageNet-1k [71] and the corresponding settings are similar to those well-established in TorchVision [72], including data augmentation, loss functions, and training methods, their parameters and schedules. For the ResNet method, we evaluate split points at blocks 3, 7, and 13, since the model is deeper.

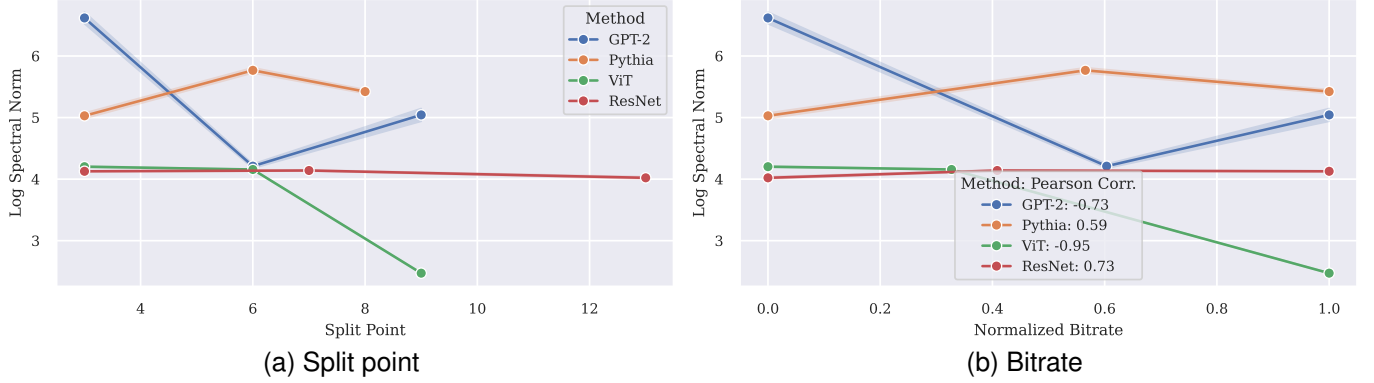


Fig. 1. Estimates of the Lipschitz constant at different split points and corresponding bitrates, for GPT-2 Small, Pythia 160M, ViT B/16 and ResNet 34. The logarithmic scale is used. Bands show the standard deviation of the estimates over 10 samples.

To adapt our entropy model to a ResNet, a convolutional layer is prepended to the entropy model so, across all split points, the resulting number of channels is $E = 768$ and the spatial dimensions are 7×7 . These dimensions are flattened out and used as input for the entropy model after learnable positional embeddings have been added. A dense layer is appended to the entropy model to recover the initial dimensionality.

The λ hyper-parameter is chosen so that the distortion obtained at subsequent split points is as close and higher than previous points. Thus, the changes in rate cannot be attributed to different distortions.

F. Lipschitz constant of the optimized entropy model

The Lipschitz constant of $r \in \mathcal{V}_r$ is approximated using the power iteration method on its Jacobian:

$$\bar{\text{Lip}}(r) = \frac{1}{N} \sum_{\mathbf{y} \in \mathcal{D}} \sqrt{b_K^\top J_r^\top(\mathbf{y}) J_r(\mathbf{y}) b_K}; \quad b_{k+1} = \frac{J_r^\top(\mathbf{y}) J_r(\mathbf{y}) b_k}{\|J_r^\top(\mathbf{y}) J_r(\mathbf{y}) b_k\|_2}, \quad (76)$$

where b_0 is initialized randomly such that $\|b_0\|_2 = 1$. Figure 1a shows these measures per split point, for $N = 100$, $K = 1,000$, and $T = 512$.

Figure 1b shows the correlation between the Lipschitz constant of the trained entropy models and the bitrate of their target representations, for each of the codecs previously evaluated. With perhaps the exception of the ViT method, the correlation between these quantities seems rather weak.